Vibrational dephasing at surfaces: The role of cubic anharmonicity and Fermi resonances

Kieron Burke* and David C. Langreth
Department of Physics and Astronomy, Rutgers University, Piscataway, New Jersey 08855-0849

Mats Persson
Department of Applied Physics, Chalmers University of Technology, S-412 96 Göteborg, Sweden

Z.-Y. Zhang
Department of Chemistry, University of California, Santa Barbara, Santa Barbara, California 93106
(Received 14 August 1992)

We make a theoretical study of the vibrational contributions to the line shape of a top-bonded adsorbate. Dephasing of the adsorbate-substrate stretch occurs via anharmonic coupling to lower-frequency modes. We find the surprising result that central forces, which are often much larger than bond-bending forces, do *not* contribute to the linewidth, due to a cancellation between cubic and quartic terms in the effective coupling to the dephasing modes. This cancellation is complete whenever the probed mode has a frequency far above all others in the system, e.g., H/Si(111) or the C-O stretch in CO on metals. The C-metal stretch in CO on metals is more complicated, as it lies well below the C-O stretch. If the CO bond is treated as rigid, the cubic term introduces Fermi-resonance effects which greatly broaden the linewidth and also give rise to extra peaks in the absorption spectrum. However, we show that the internal motion of the molecule, no matter how small, causes a dramatic reduction in the magnitude of these effects, probably rendering them unobservable. We suggest that one must look to anharmonic terms in the noncentral (bending) interatomic forces to explain the magnitude of the experimental dephasing linewidth.

I. INTRODUCTION

When an atom or molecule is adsorbed on a surface, several additional vibrational normal modes are introduced which are directly associated with the bonding to the surface. The field of vibrational spectroscopy has mainly concentrated on what can be learned about the adsorbate-substrate bond from studies of the peak positions of the frequency spectra of such modes. It is only recently that infrared techniques have achieved sufficient resolution and signal to noise to study the detailed shapes of the spectra of adsorbate-substrate stretch modes. The present paper deals primarily with the shape of such a dipole active spectrum and how it is affected by the anharmonicity of the adsorbate-substrate bond. We also attempt to answer the inverse issue: what can one learn about the interatomic forces by a study of the shape of this spectrum in the vicinity of the adsorbate-substrate stretch?

We consider here the simplest case of an adsorbate on a top site in which the normal modes may be divided into two classes that do not couple (in the harmonic approximation): those with the same symmetry as the perpendicular and parallel adsorbate motion, respectively. We also restrict ourselves to systems where the frequency of the adsorbate-stretch mode is located well outside the substrate phonon band. The adsorbate-substrate stretch mode is called the "A" mode in the case of an atomic adsorbate and the "M" mode in the case of a molecular adsorbate. In this case it has been shown[1,2] that anharmonic coupling of the A or M modes to the other substrate modes with the same symmetry as the perpendicular adsorbate modes has a negligible effect, so that one is left with the theoretical problem of an oscillator coupling anharmonically with a field of oscillators of different symmetry. That these conditions are not very restrictive is demonstrated by the fact that there have already been several experimental studies of such systems. Dumas, Chabal, and Higashi[3] have measured the A mode of atomic H adsorbed on the (111) surface of Si. The M mode of molecular CO adsorbed on Pt(111) has also been extensively studied[1,4,5] and CO/Ni(100) is currently being studied,[6] although there also exists earlier work.[7]

We begin in the next two subsections by introducing the problems, or rather the apparent contradictions, with experimental observations that arise when trying to model the anharmonicity of the molecular-substrate bond with a central force field. In the third subsection, we present the main results in a physically intuitive and transparent way. These not only resolve the above problems for a diatomic adsorbate, but also give an unexpected prediction for the monatomic one. In the final subsection, we given an outline of the sections in the paper in which these results are derived in detail using many-body diagrammatic perturbation theory.

A. Why are Fermi-resonance effects typically *not* observed for diatomic adsorbates?

In order for this question to make sense we first give a convincing argument for why one might expect to see Fermi-resonance effects in the dipole spectrum in the vi-

cinity of the M mode. To do this we must consider all the adsorbate-induced modes. We focus on the case of CO adsorbed on various transition metals where CO lies on an axis perpendicular to the surface with C inward, as there exists sufficient experimental data for this case. Figure 1 is an illustration of such a case, indicating the motions of the C and O atoms in the various modes, while Fig. 2 illustrates the assumed density of states of normal modes of the complete system.[8] The frequency ω_M of the M mode is typically between 400–500 cm^{-1}, while the other perpendicular mode, consisting principally of the internal stretch of the CO molecule, which we term the I mode, typically has a frequency over 2000 cm^{-1}. Both of these are true normal modes of the system, since they both lie above the phonon continuum. It usually lies between 0 and about 300 cm^{-1} or less, and we denote its highest frequency by ω_{max}. The difference between the frequencies is sufficiently large that the force constant for the M mode is almost one order of magnitude smaller that for the I mode. This implies that the M mode is indeed as we described it, essentially a rigid stretch of the metal-CO bond, with only a small fixing of the internal bond. This flexing is thus customarily neglected in line-shape calculations of the type described here. The parallel modes of the molecular adsorbate are often termed a frustrated rotation R and a frustrated translation T. The latter typically has a very low frequency ω_T of 50 cm^{-1} or less. It is not a true normal mode, because there is an admixture of substrate phonons, but this admixture is small because the phonon density of states is necessarily small at such small frequencies. We term it a quasimode, describable by a frequency ω_T and a much smaller width or inverse lifetime γ_0. In contrast the R mode typically has a frequency ω_R comparable to, but a bit less than, that of the M mode and lies above the continuum. Note that because of the high adsorption site symmetry, and two R modes and the two T modes are degenerate and uncoupled for each direction parallel to the surface, and in what follows we only talk about a given pair.

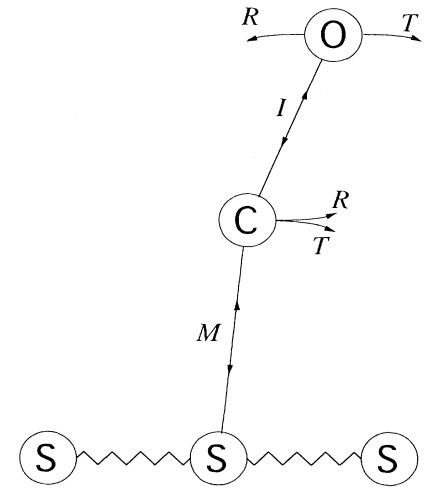

FIG. 1. Schematic of CO atop a metal substrate, illustrating the principal atomic motions in the various modes (T,R,M,I) described in the text. The associated substrate motions have not been indicated.

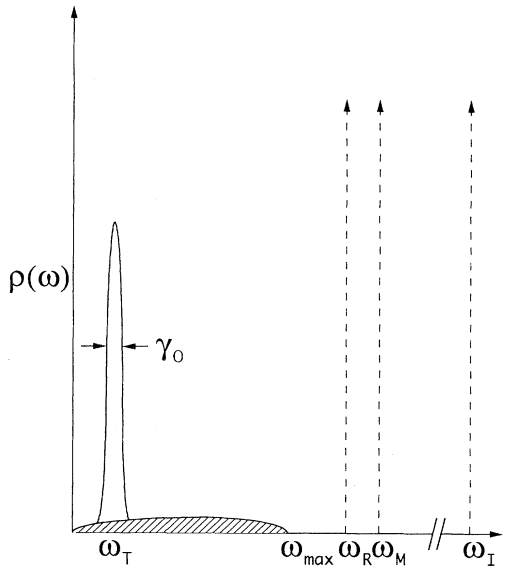

FIG. 2. Schematic density of states of normal modes of the coupled adsorbate-substrate system shown in Fig. 1. The arrows indicate truly localized modes which have δ-function densities, while the hatched area is the phonon continuum.

The values of these mode frequencies for several surfaces are listed in Table I. Note that in all cases the frequency difference $\omega_M-\omega_R-\omega_T$ is quite small in comparison with ω_M. This represents a typical Fermi-resonance situation where one can, through dipole coupling, excite the linear combination ω_R plus ω_T as well as ω_M, exploiting a small energy denominator in a second-order matrix element. Of course, to do this requires the presence of sufficiently large anharmonic terms with the right symmetry; we next argue that such terms are *always present.*

The energy required to stretch the C-metal bond is $\frac{1}{2}k(l-l_0)^2$ plus higher-order terms. Here, l_0 is the un-

TABLE I. Observed vibrational frequencies and binding parameters for top-bonded CO on some metal surfaces. All frequencies are in units of cm^{-1}. Data are taken from a, Ref. 18; b, Ref. 19; c, Ref. 20; d, from (b) and consistent with data in (i); e, Ref. 21; f, Ref. 22; g, Ref. 23; h, extrapolated; i, Ref. 24; j, Ref. 25; k, Ref. 26; l, Ref. 27; m, derived in LP; n, Ref. 28; o, Ref. 1; p, Ref. 29.

	Pt(111)	Cu(100)	Ni(100)	Ir(100)
ω_{max}	183[a]	242[a]	306[a]	229[k]
ω_T	49[b]	28[f]	26[l]	53[j]
ω_R	410[c]	285[g]	(380)[m]	425[j]
ω_M	460[o]	345[g]	475[n]	497[j]
ω_I	2100[c]	2090[e]	2069[p]	2068[j]
l_{0I} Å	1.16[b]	1.15[i]	1.15[d]	(1.16)[h]
l_{0M} Å	2.05[b]	1.9[i]	1.84[d]	(1.99)[h]

stretched bond length and l is the actual instantaneous value

$$(l-l_0)^2=[\sqrt{(l_0+z)^2+x^2}-l_0]^2 \approx z^2+x^2z/l_0+\ldots , \quad (1.1)$$

where x and z refer to directions parallel and perpendicular to the surface, respectively. The last term in (1.1) has the required symmetry, and gives rise to the interaction Hamiltonian

$$H_{x^2z}=\frac{k}{2l_0}x^2z=\frac{M_M\omega_M^2}{2l_0}x^2z , \quad (1.2)$$

where M_M is an effective mass for the M mode ($\approx$28 amu, a bit less for the less massive substrates). Terms similar to (1.2) also arise from the noncentral or bond-bending forces, but these are expected to be an order of magnitude smaller because of the much smaller bending force constants.

The matrix element connecting the state containing one M excitation and the state containing one T and one R excitation is now easily estimated by expanding x and z in (1.2) in approximate normal modes,

$$x=(M_T)^{-(1/2)}q_T+(M_R)^{-(1/2)}q_R , \quad (1.3a)$$

$$z=(M_M)^{-(1/2)}q_M , \quad (1.3b)$$

where the q's are the amplitudes of the canonical (mass-weighted) normal coordinates (approximate, in the case of q_T). Because $\omega_R \gg \omega_T$ we know that the T mode must consist approximately of a rigid rotation of the substrate-C-O atoms in a line, in order to avoid the bending of a bond with a stiff bending constant. Assuming a rigid substrate, the mass M_T is that mass which, when placed at the C position, would give the same moment of inertia as that of the actual arrangement. Using the data of Table I one finds for all surfaces listed that this is $\approx 4M_C$ or around 50 amu. This means that in this projection the T mode is getting around $\frac{1}{4}$ of the weight, so that the R mode gets around $\frac{3}{4}$ giving $M_R \approx \frac{4}{3}M_C$ or around 16 amu. State-of-the-art calculations do not change these numbers substantially. Upon substitution of (1.3b) in (1.2), the matrix elements of H_{x^2z} between the appropriate oscillator states can be written down by inspection as

$$\langle TR|H_{x^2z}|M\rangle=\left[\frac{M_M\omega_M^3}{8l_0^2M_RM_T\omega_R\omega_T}\right]^{1/2} , \quad (1.4)$$

where $|M\rangle$ is the state with one quantum in the M oscillator and none in the other two, while $|TR\rangle$ is the state with one quantum in each of the T and R oscillators and none in the M. Thus, one needs only to solve a 2×2 problem with the result that a second spectral line in addition to the original or M mode line should be excited. The strength ratio of this line relative to the "original" is given in terms of the parameter $r\equiv|\langle TR|H_{x^2z}|M\rangle/(\omega_M-\omega_R-\omega_T)|$ by r^2 when r is small and *unity* when r is large. The second line is at the position $\omega_R+\omega_T$ when r is small, but as r increases the lines repel so that the minimum splitting is $2|\langle TR|H_{x^2z}|M\rangle|$. The actual calculated strength ratios from the data in Table I are given below. [For the reader's convenience we note that the conversion factor from $(\text{amu})^{-1}\text{Å}^{-2}$ to frequency in cm^{-1} is 33.5.]

	Pt(111)	Cu(100)	Ni(100)	Ir(100)
Strength ratio	0.93	0.14	0.08	0.28

These numbers illustrate that one should see Fermi-resonance effects in most of these adsorption systems.

This "prediction" arises from a term in the Hamiltonian that is unquestionably present, and the estimate of whose magnitude comes from very general arguments which are very unlikely to be qualitatively incorrect. Yet the fact is that these "predicted" Fermi-resonance effects are not seen experimentally. The solution to this dilemma is one of the principal results of this paper.

B. Why is the dephasing width of the M mode so small?

The temperature-dependent line shape of the M mode should generally be controlled by dephasing processes, which can be thought of as thermal fluctuations in the frequency of ω_M. The quasimode T is expected to dominate this dephasing process because of its sharpness along with the fact that it can be thermally excited in the experimental temperature range. Thus, n_T, the instantaneous quantum number of the T mode, is expected to be the dominant fluctuating variable in the dephasing process. In principle, two-phonon emission and absorption could also be a contributor to the temperature-dependent line shape, but because of the requirement of energy conservation, a significant contribution would require the accidental coincidence of there being peaks in the appropriately projected phonon density of states at two frequencies that add up to ω_M (or one peak at $\omega_M/2$). Therefore, we do not expect such a contribution here.

In lowest-order perturbation theory dephasing arises because the quartic terms (or more precisely biquadratic x^2z^2 terms) in the Hamiltonian change the spacing between the oscillator levels of the M mode, and at finite temperatures this spacing is a fluctuating quantity. Terms of this type can come from higher-order terms in the expansion of (1.1),

$$H_{x^2z^2}=-\frac{k}{2l_0^2}x^2z^2=-\frac{M_W\omega_M^2}{2l_0^2}x^2z^2 . \quad (1.5)$$

To lowest order the shift in the frequency of the M mode is

$$\Delta\omega_M=\langle Mn_T|H_{x^2z^2}|n_TM\rangle-\langle n_T|H_{x^2z^2}|n_T\rangle , \quad (1.6)$$

where $|n_TM\rangle$ is the state with one M quantum and n_T T quanta, while $|n_T\rangle$ is the state with no M quanta and n_T T quanta. Using (1.3b) and (1.5), (1.6) can be evaluated by inspection yielding

$$\Delta\omega_M=\lambda_0(n_T+\tfrac{1}{2}) , \quad (1.7)$$

where

$$\lambda_0 = -\frac{\omega_M}{2l_0^2 M_T \omega_T} . \tag{1.8}$$

Here, λ_0 is the change $\Delta\omega_M$ for a unit change in the fluctuating variable n_T and is by definition the coupling constant for the dephasing problem, as it is the thermal fluctuations in this shift that cause dephasing.

The exact solution of the dephasing of the M mode due to biquadratic coupling of the type (1.5) with a T quasimode was accomplished previously by two of us.[2] Using (1.8) we then gave a solution free from adjustable parameters. Reasonable agreement with experiment for CO/Pt(111) was found over the whole temperature range, the only system for which there was such data. Very rough agreement was also found with the single experimental point for CO/Ni(100).

So, what is the problem? It arises because the term proportional to $(l-l_0)^3$ in the Taylor expansion of the C-metal bond-stretching energy [see text above (1.1)] also makes a contribution to the x^2z^2 term in the Hamiltonian. Therefore, (1.5) is not complete. Of course the coefficient of $(l-l_0)^3$ is not known exactly, but a reasonable estimate of it may be made by fitting a Morse potential (or another reasonable two-parameter form) to the experimental values of ω_T and the well depth. The result is that one's best estimated value of $H_{x^2z^2}$ is roughly *an order of magnitude larger* than the value in what we call the minimum anharmonicity model, (1.5). This is in contrast to the situation with H_{x^2z} for which there are no such corrections to (1.2). The result is that the predicted dephasing line shape was more than an order of magnitude larger than experiment.[2] So we are faced with the question of why what seemed the most physically reasonable model gave nonsense. The solution to this dilemma is another of the chief results of this paper.

C. Procedure and results

1. Cubic terms

The answer to part of the dephasing puzzle comes from the inclusion of cubic terms. It has been shown[9,10] for the perpendicular modes that if one made second-order matrix elements out of cubic terms one could obtain dephasing contributions that were of the same order of magnitude as the quartic contributions. However, in that particular case the effect was quantitative, but not qualitative, and the matter was dropped when the renormalization that made the effect of the perpendicular modes negligible was discovered.[1,2] In Sec. III we show that the cubic terms are important for dephasing by parallel modes, and that here they have an important *qualitative effect.* The reason that we were able to obtain an essentially exact solution is that $\omega_T/\omega_M \ll 1$ with these quantities differing by an order of magnitude. We find to leading order in this ratio that the effective dephasing coupling constant is

$$\lambda_{\text{eff}} = \lambda_0 \left[1 - \frac{M_M}{M_B}\right] + \lambda_{\text{Fermi}} , \tag{1.9}$$

where λ_{Fermi} is a contribution coming from the various possible Fermi resonances which will be discussed a bit later. The quantity M_B is a combined effective mass for all low-energy parallel modes (T plus phonons). It is approximately equal to M_T; in the approximation (1.3b) this approximate equality becomes exact.

The above equation already includes two important results of this paper. The first is that all the terms involving higher-order stretching force constants, such as the coefficient of the $(l-l_0)^3$ term in the bond-stretching energy, have cancelled out. This means that *only the quadratic terms in the bond-stretching energy are important for dephasing.* It also means that the "minimal anharmonicity model" is exact, provided that the coupling constant λ_0 in the Langreth-Persson theory[2] is replaced in that theory by λ_{eff}. The second important result occurs when we specialize in the case of a monatomic adsorbate. In that case $\lambda_{\text{Fermi}}=0$ and $M_M=M_B=M_A$ and one obtains the remarkable result that $\lambda_{\text{eff}}=0$. This means that *the stretching of the adsorbate-substrate bond does not give rise to any dephasing in the case of a monatomic adsorbate.* Whatever dephasing that exists in this case must come from the much smaller noncentral bond-bending forces. The physics of this remarkable result is discussed via a simple example in Sec. III C 3.

Returning to the diatomic adsorbate case, there are still problems. The introduction of cubic terms cures one problem but introduces two more: first, it predicts unobserved Fermi resonances already discussed, and second these resonances cause a large unobserved enhancement in the dephasing coupling constant through λ_{eff}. Here we give a simplified version of our results on this second point to facilitate the discussion of the physics.

The presence of a Fermi resonance can cause the term λ_{Fermi} to be large, because the shift of the resonance frequency is dependent on the fluctuating variable n_T. To see this we must recalculate the matrix element (1.4) in the presence of an initial nonzero value for this variable. This is easily done with the result that the right side of (1.4) should be multiplied by $\sqrt{n_T+1}$. Then solving the 2×2 for the eigenvalues gives the frequency shift of the M mode due to this mechanism,

$$\Delta\omega_{\text{Fermi}} = \tfrac{1}{2}[\sqrt{(\omega_M-\omega_R-\omega_T)^2+\delta\omega_M^2} - (\omega_M-\omega_R-\omega_T)] , \tag{1.10}$$

where here and in (1.12) below the radical sign denotes that square root that has the same sign as the quantity $(\omega_M-\omega_R-\omega_T)$ and where

$$\delta\omega_M^2 = \frac{M_M\omega_M^3}{2l_0^2 M_R M_T \omega_R \omega_T}(n_T+1) . \tag{1.11}$$

The contribution to λ_{Fermi} is then

$$\lambda_{\text{Fermi}} = \frac{\partial \Delta\omega_{\text{Fermi}}}{\partial n_T} = -\lambda_0 \frac{M_M \omega_M^2}{4 M_R \omega_R} \frac{1}{\sqrt{(\omega_M - \omega_R - \omega_T)^2 + \delta\omega_M^2}} \, . \tag{1.12}$$

This expression still contains the fluctuating variable n_T through the $\delta\omega_M$ term in the square root, so that one has not obtained a meaningful coupling constant unless (i) one is sufficiently far from the Fermi resonance that the $\delta\omega_M$ term can be neglected, or (ii) it is valid to replace n_T by its average thermal value; the latter is the case if the resulting coupling constant is small enough to make lowest-order perturbation theory valid. We also mention that there are smaller nonresonant contributions to $\Delta\omega_{\text{Fermi}}$ that we omit in this section so as not to obscure the essential argument. The central result is that there is a large increase in the dephasing coupling constant because the M mode frequency is a rapidly varying function of the fluctuating variable n_T near a Fermi resonance.

Using the data in Table I in Eq. (1.12), one obtains values of λ_{Fermi} that are an order of magnitude larger than the minimum harmonicity model value (λ_0). Such values would imply dephasing linewidths nearly two orders of magnitude larger than those consistent with experiment.

2. *The role of internal C-O bond*

We believe that the theory summarized above and detailed in Sec. III coupled with the work of Ref. 2 represents essentially the exact solution to the model presented, and that the violent disagreement with experiment in the case of a diatomic adsorbate means that a new starting point must be invoked. The new physics came upon the realization that the standard arguments for the neglect of the internal stretching of the molecule when considering the M mode need to be modified in one important respect. It is indeed true that the stretching z_I of this bond is small relative to the stretching z_M of the M mode, that is $z_I \propto (k_M/k_I) z_M$, where the k's are the appropriate force constants whose ratio differs by almost an order of magnitude. This means that in all harmonic terms and most anharmonic terms the internal stretch motion is negligible. However, cubic terms of the type (1.2) applied now to the internal mode are no longer negligible. In this type of term that has exactly *one* power of z_I, the smallness of z_I is exactly balanced by the largeness of the k_I out front. *Thus, no matter how stiff the internal stretch is, no matter how small the internal stretch motion is, it must be included to avoid throwing away terms that are formally as important as those that come from the M mode stretch.*

One might perhaps be discouraged from pursuing this avenue as a possible solution to the Fermi-resonance dilemma, because while it introduces considerable complexity, one expects it to produce only small quantitative changes. One should now expand the sum of *two* terms such as (1.2) in normal coordinates and calculate the matrix element analogous to (1.4). In the frozen lattice approximation with widely separated frequencies ($\omega_I \gg \omega_M$; $\omega_R \gg \omega_T$) this may be done analytically, and one finds that this matrix element is (1.4) multiplied by a geometric factor and a mass ratio factor. Although each of these factors could be considered of order unity, the overall result is a major change. More quantitatively, the mass ratio factor is $\approx \frac{1}{2}$ and the geometric factor is $\approx \frac{1}{3}$, and since the matrix element is always squared, the overall effect of these factors is to reduce the importance of the Fermi resonance in this problem by a factor of $\frac{1}{40}$ or so. One obtains a new set of strength ratios analogous to the bare strength ratios given above.

	Pt(111)	Cu(100)	Ni(100)	Ir(100)
Strength ratio	(see text)	0.005	0.003	0.013

Thus, in at least three out of four cases the Fermi resonance is probably too weak to be seen. In the case of Pt, the frequencies are so close to resonance that the predicted value is extremely sensitive to the exact values used; the experimental values for the frequencies are not sufficiently accurate to predict this case with any reliability. For example, if we use $\omega_R = 410$ cm^{-1} we obtain a strength of 0.61, but if we use 420 cm^{-1}, we obtain a strength of 0.044. In Sec. IV the calculation was performed via a correlation function method, where it was unnecessary to make the rigid lattice and widely separated frequency approximation. The results predict even larger strength reductions than for the simple analytic model.

Calculations of the dephasing line shape were also carried out for this model where the internal stretch is taken into account. The first important result is that the minimum anharmonicity model is still exact, that is the large anharmonic coefficients arising from bond-stretching energies of the form $(l - l_0)^3$ still completely cancel out of the expression for the dephasing coupling constant of a high-frequency M mode. The second important result is implied by the Fermi-resonance reduction discussed above: λ_{Fermi} in Eq. (1.12) is renormalized by multiplying the numerator of the right side (as well as the $\delta\omega_M$ in the square root) by the reduction factor ($\approx \frac{1}{40}$ in the analytically solvable model). Finally, the non-Fermi part of the effective coupling constant [the first term in Eq. (1.9) for λ_{eff}] also gets reduced. This too is typically a substantial reduction of approximately a factor of $\frac{1}{20}$. Thus, one is left with $|\lambda_{\text{eff}}| \ll |\lambda_0|$, which means that central forces are not responsible for the observed line shapes, and presumably noncentral forces need to be invoked to explain experimental results.

D. Outline of paper

In Sec. II we introduce the basic Hamiltonians that will be used throughout the paper: First, the harmonic Hamiltonian for a monatomic adsorbate case and then a

diatomic adsorbate case; then the anharmonic terms that come from stretching a single bond, terms which apply to each of the subsequent sections.

Section III gives the solution to monatomic adsorbate case and also to the case of a diatomic adsorbate where only a single bond is allowed to stretch, thus including everything discussed through Sec. I C 1 of this introduction. After further introduction to the notion of dephasing in Sec. III A, we outline the calculation of the renormalized coupling constant in Sec. III B via a full many-body calculation of the correlation function directly related to the experimental measurement; the renormalized coupling constant appears in the form of an effective vertex in the expansion of this correlation function, and we show for a high-frequency M mode that this procedure is exact. In Sec. III C we specialize these results to the monatomic adsorbate case and in addition give a simple example that explains the physics of why there is no dephasing from bond stretching in this case. Finally, in Sec. III D we include the high-frequency R mode in our formalism and derive the results in the presence of a Fermi resonance.

In Sec. IV we generalize the previous results to the case where the stretching of both bonds is allowed. Section IV A explicitly generalizes the Hamiltonian to cover this case. Sec. IV B 1 introduces and calculates the necessary generalizations of the correlation functions in the harmonic approximation. In Sec. IV C we apply them to the calculation of the Fermi resonance, finding that it renormalized as discussed above. In Sec. IV D we are able to generalize the effective vertex results to the case where both bonds stretch, and derive the dephasing coupling constant in this model as discussed above. Finally, in Sec. IV E we apply our results to the materials in Table I.

II. HAMILTONIAN

In this section, we define the harmonic part of the Hamiltonian for this problem. We begin with the case of an atomic adsorbate, and follow with that of a diatomic adsorbate. We then define the anharmonic contribution to the Hamiltonian, but only for the case of a single anharmonic bond. For a diatomic molecule, the single-bond anharmonic model means not allowing the internal stretch to move. We stress here that this model for the dephasing of a diatomic adsorbate is incomplete, as is shown by our results of Sec. III, and we develop a complete model for the diatomic case in Sec. IV.

A. Harmonic approximation for atomic adsorbate in a top site

We consider the general situation of having an adsorbate-substrate stretch (AS) of an atomic adsorbate in an on-top site. A prime example of such a system is H on Si(111) but we also later investigate to what extent the stretch modes of a molecular adsorbate such as CO can be reduced to this situation.

The symmetry of an atomic adsorbate in a top site makes the motion perpendicular and parallel to the surface decouple in the harmonic approximation, and we can decompose H_{harmonic} as

$$H_{\text{harmonic}}=H_{\perp}+H_{\parallel} . \tag{2.1}$$

The adsorbate-substrate stretching vibration and substrate modes coupled to it are all included in $H_{\perp}$. We assume that the AS vibrational frequency is determined by a central force between the adsorbate and the nearest-neighboring substrate atom and $H_{\perp}$ is given by

$$H_{\perp}=\frac{p_{1,z}^2}{2M_A}+\tfrac{1}{2}k_A(z_1-z_2)^2+H_{\perp}^{\text{substrate}} , \tag{2.2}$$

where the subscripts 1 and 2 refer to the adsorbate and substrate atoms, respectively, and z is the coordinate perpendicular to the substrate. In the frozen substrate situation, the AS vibrational frequency $\omega_A^{(\infty)}$ is simply determined from the force constant k_A as $k_A=M_A\omega_A^{(\infty)2}$. In all situations of interest in this paper, $\omega_A^{(\infty)}$ is typically much larger than the maximum substrate phonon frequency $\omega_{\max}$ which makes the displacement field of the AS mode closely correspond to a bond stretch even when coupled to the substrate modes. This behavior is best understood from an analysis of the correlation function $L_{\perp}^h$ for z_1-z_2 in the harmonic approximation as defined by Langreth and Persson (hereafter referred to as LP).[2] The localized AS mode gives rise to a pole in $L_{\perp}^h$ and near this pole one finds that

$$L_{\perp}^h(\omega)=\frac{1}{\mu_{\perp}}\frac{Z_A}{\omega^2-\omega_A^2} , \tag{2.3}$$

where $\mu_{\perp}$ is the reduced mass of the adsorbate and the substrate atom

$$\frac{1}{\mu_{\perp}}=\frac{1}{M_A}+\frac{1}{M_S} . \tag{2.4}$$

The coupling to the substrate modes shifts the vibrational frequency $\omega_A^{(\infty)}$ in the frozen substrate situation up to ω_A and to leading order in $(\omega_{\max}/\omega_A)^2$,

$$\omega_A^2=\left[1+\frac{M_A}{M_S}\right]\omega_A^{(\infty)2} . \tag{2.5}$$

The spectral strength Z of the mode is in this high-frequency limit bounded below by

$$1-\frac{M_A}{M_S+M_A}\frac{\omega_{\max}^4}{\omega_A^4}\le Z_A\le 1 . \tag{2.6}$$

In most situations of interest in this paper $\omega_A\gg\omega_{\max}$, the strength Z_A is then very close to unity and exhausts the zero-moment sum rule and this fact together with the result for ω_A in (2.5) illustrates that the AS mode is well localized to the adsorbate and the nearest-neighboring substrate atom.

In the situation of adsorbate modes polarized parallel to the surface, noncentral forces are needed for nonzero vibrational frequencies. For instance, noncentral forces can be modeled by a simple valence force field as

$$H_{\parallel}=\frac{p_x^2+p_y^2}{2M_A}+\tfrac{1}{2}B\theta^2+H_{\parallel}^{\text{substrate}} , \tag{2.7}$$

where the bending angle θ is the deviation of the AS bond

axis from the surface normal, B is the associated bending force constant, and x and y are the coordinates parallel to the surface. Typically, angle-bending forces are much smaller than central forces. For instance, the H-Si stretch frequency of 2084 cm^{-1} as compared to 637 cm^{-1} for its parallel mode gives almost a factor of 10 difference between the restoring force constants K_A and B/l_0^2, where l_0 is the AS equilibrium distance. Note that the low mass of H compared to that of Si makes the adsorbate vibrational frequencies for a frozen substrate negligibly different from those for a dynamic substrate. In this work we make frequent use of the fact that the high symmetry of the on-top site in (111) and (100) surfaces makes the parallel modes in $H_\parallel$ doubly degenerate and it is sufficient to consider modes along only one direction, e.g., the x direction.

B. Harmonic approximation for top-bonded CO

As we stressed in the Introduction the adsorbate modes of top-bonded CO show a very similar behavior on many metal surfaces as can be seen from Table I. We model these vibrational modes and the substrate modes by a minimal force-constant model introduced by Leiro and Persson[11] (hereafter referred to as JP) for bridge-bonded CO molecules and later extended by LP to top-bonded molecules. In order to have an easy reference, we explicitly introduce here the details of this force-constant model for the molecular adsorbate while the details of the substrate force field are not important and the reader is referred to LP or JP.

The high symmetry of the CO molecule adsorbed on a top site on the (100) and (111) surfaces is as high as for an atomic adsorbate and the decomposition in (2.1) of the H_{harmonic} still applies. The perpendicular adsorbate modes are assumed to be determined by central force constants as

$$H_\perp=\frac{(p_{1,z})^2}{2M_C}+\frac{(p_{0,z})^2}{2M_O}+\tfrac{1}{2}k_M(z_1-z_2)^2 +\tfrac{1}{2}k_I(z_0-z_1)^2+H_\perp^{\text{substrate}} , \tag{2.8}$$

where the subscripts 0,1 now refer to the O and C atoms, respectively. The high vibrational frequency of the I mode compared to the frequency of the M mode suggests that the changes in the C-O separation can be assumed to be small at the frequency of the M mode and we can make the pole approximation in (2.3) for this mode but now with $M_A=M_C+M_O$ and $k_A=k_M$. In a later section we will see that while this is a good approximation for the vibrational frequency, the approximation that the C-O separation is rigid is not valid in the modeling of the anharmonicity. We have checked all these approximations for CO on Pt(111) by numerically calculating the adsorbate vibrational frequencies by fitting k_I and k_M to the observed frequencies in Table I,

	(M)	(I)
k_λ (mdyn/Å)	3.24	16.65

[For the reader's convenience, we note the conversion 1 mdyn/Å $=1.697\times10^6$ cm^{-2} amu].

In order to have a nonzero frequency of the modes parallel to the surface it is also necessary in this situation to have noncentral forces. Here, these forces are modeled by angle-bending force constants as

$$H_\parallel=\frac{(p_{1,x})^2+(p_{1,y})^2}{2M_C}+\frac{(p_{0,x})^2+(p_{0,y})^2}{2M_O} +\tfrac{1}{2}B_R\theta_R^2+\tfrac{1}{2}B_T\theta_T^2+H_\parallel^{\text{substrate}} , \tag{2.9}$$

where B_R and B_T are the bending force constants associated with the bending angles θ_R and θ_T. The angle θ_T is the deviation of the angle of the bond axis C-S from the surface normal and $\pi+\theta_R$ is the angle between the bond axes S-C and C-O.[11]

In the frozen substrate situation $H_\parallel$ in (2.9) gives rise to two doubly degenerate adsorbate modes denoted by T and R with frequencies $\omega_R^{(\infty)}$ and $\omega_T^{(\infty)}$, respectively. The frequency $\omega_T^{(\infty)}$ of the mode T is well below $\omega_{\max}$ and acquires a small shift and broadens into a narrow resonance when coupled to the substrate modes while the mode R with a frequency $\omega_R^{(\infty)}$ well above $\omega_{\max}$ shifts upwards in frequency and is still localized. These effects have been calculated in LP by adjusting the bending force constants B_T and B_R to the observed frequencies,

	(T)	(R)
B_λ (mdyn/Å)	0.33	0.47

Also, in this case the angle-bending force constants $B_T/l_{0M}^2=0.08$ mdyn/Å and $B_R/l_{0I}^2=0.35$ mdyn/Å are much less than the stretching force constants k_M and k_I above.

In general, the correlation function $L_\parallel^h$ for x_1-x_2 in this situation has exactly the form

$$L_\parallel^h(\omega)=L_\parallel^{h,\text{band}}(\omega)+\frac{Z_R}{\mu_\parallel(\omega^2-\omega_R^2)} , \tag{2.10}$$

thus separating out the discrete normal mode at ω_R from the continuous band part. Here, ω_R is the frequency of the frustrated rotation or R mode and Z_R its spectral strength, and where

$$\frac{1}{\mu_\parallel}=\frac{1}{M_C}+\frac{1}{M_S} . \tag{2.11}$$

The effective mass M_R introduced earlier is related to Z_R by the relation $Z_R=\mu_\parallel/M_R$. Similarly, if we introduce a weight for the continuous band spectrum $Z_B\equiv1-Z_R$, then the effective mass M_B is given $Z_B=\mu_\parallel/M_B$. The above are exact quantities. However, the calculations above show that this band part may be adequately represented by a single pole representing the T mode with only a negligible amount of weight (several percent) left over for the rest of the continuum band (phonons). The resulting correlation function $L_\parallel^h$ for x_1-x_2 can therefore be well approximated by the two-pole approximation and may be written (for $\text{Im}\omega>0$) as

$$L_{\parallel}^{h}(\omega)\approx\frac{Z_T}{\mu_{\parallel}[(\omega^2-\omega_T^2)+i\omega\gamma_0]}+\frac{Z_R}{\mu_{\parallel}(\omega^2-\omega_R^2)}\ , \tag{2.12}$$

where ω_T, γ_0, and Z_T are the frequency, width, and strength of the bending resonance T. The mass M_T introduced earlier is defined in terms of Z_T as $Z_T=\mu_{\parallel}/M_T$. The above representation is approximate. That it is a good approximation is demonstrated by the fact that the sum of the calculated spectral strengths in Table IV as shown below is close to unity.

Finally, the good quality of the bending force-constant model for the parallel modes is demonstrated by its application to the observed isotope shifts of the mode R of CO on Cu(100). This model gives the isotope shifts $\Delta\omega_R^{\text{theory}}$ for the R mode $C^{12}O^{18}$ which should be compared with the observed shifts $\Delta\omega_R^{\text{exp}}$ by Hirschmugl *et al.*,[12]

	$\Delta\omega_R^{\text{theory}}$	$\Delta\omega_R^{\text{exp}}$ cm^{-1}
$C^{12}O^{18}$	-3	~ 0
$C^{13}O^{18}$	-12	-12

As can be seen from this comparison the agreement is good.

C. Anharmonicity of a single bond

Here we use the same anharmonic model as developed in LP which assumes that the anharmonicity derives solely from the central force associated with the bond stretch. From the presentation in the two previous subsections this model is motivated by the following two observations: (i) the displacement fields for the perpendicular adsorbate modes correspond primarily to a bond stretch, and (ii) the force field is dominated by its central part. The potential $U(l)$ of this force then depends only on the bond distance l. The perpendicular and parallel components of $l-l_0$ are denoted by z and x, respectively. In the case of the stretch mode M and for the molecular mode I, l is the C-S and the C-O separation, respectively, and $x=x_1-x_2$ and $z=z_1-z_2$, and $x=x_0-x_1$ and $z=z_0-z_1$, respectively. We expand $U(l)$ about its minimum at $l=l_0$,

$$U(l)=K_2(l-l_0)^2+K_3(l-l_0)^3+K_4(l-l_0)^4+\ldots\ , \tag{2.13}$$

Here, $K_2=k_A/2$ in the case of the atomic adsorbate and $K_2=k_M/2$ and $K_2=k_I/2$ for the stretch modes M and I of the CO molecule, respectively. The anharmonic part $H_{\text{int}}=H-H_{\text{harmonic}}$ of the Hamiltonian H for the adsorbate-substrate is obtained by expanding $U(l)$ up to fourth order in x and z,

$$H_{\text{int}}=K_4^{\parallel}x^2z^2+K_3^{\parallel}x^2z+K_4^{\perp}z^4+K_3^{\perp}z^3\ , \tag{2.14}$$

where the quadratic terms have been incorporated in H_{harmonic}. We only write this series up to fourth order, as estimates of higher-order terms yield vanishingly small contributions. The anharmonic force constants are then given by

$$K_4^{\parallel}=\frac{(3K_3l_0-2K_2)}{2l_0^2}\ , \tag{2.15a}$$

$$K_3^{\parallel}=\frac{K_2}{l_0}\ , \tag{2.15b}$$

$$K_4^{\perp}=K_4,\quad K_3^{\perp}=K_3\ . \tag{2.15c}$$

Note that $K_3^{\parallel}$ depends only on the harmonic part of the central force. Since it is hard to calibrate the intrinsic anharmonicity of U, it is instructive to introduce a minimal anharmonicity model defined as one in which only the quadratic term in (2.13) is kept, $K_3\equiv K_4\equiv 0$.

III. DEPHASING IN THE SINGLE-BOND ANHARMONIC MODEL

In this section, we first restate the results derived by LP in their treatment of dephasing by an anharmonic Hamiltonian which contains only biquadratic terms. We then demonstrate that, although cubic terms contribute significantly to dephasing in this model, they can usually be treated as an effective quartic interaction, and the results of LP may therefore be generalized to include them. This demonstration is at the heart of all the calculations in this paper. In Sec. III C, we discuss dephasing in three special cases: by a monatomic adsorbate, by the internal CO stretch, and by a simple model, designed to illustrate why there is no dephasing in the monatomic case. Finally, in Sec. III D 1 we discuss the possibility of Fermi-resonance effects for CO, giving an estimate of the weight of a second line which in principle could appear. We also show how the single-bond model yields absurd results for realistic diatomic systems, leading us directly to Sec. IV, where a more complete model is treated.

A. Dephasing

In this paper, we consider the dephasing of the stretch modes of an atomic adsorbate and also of an adsorbed CO molecule in the high adsorbate frequency limit, i.e., $\omega_{\max}\ll\omega_M$, where $\omega_{\max}$ is the largest frequency of phonons causing dephasing and ω_M is the stretch frequency of interest. This high-frequency limit is often a good approximation and is well satisfied for the systems studied here. One important simplification in the treatment of the effects of anharmonicity on the line shape in this limit is that perpendicularly polarized phonon modes do not contribute to the line shape.[1,2] Furthermore, the line-shape problem has been solved in this limit for $H_{\text{int}}=K_4^{\parallel}x^2z^2$ by Langreth and Persson[2] for arbitrary coupling strengths in the case of dephasing by a quasimode.

In particular, in the weak-coupling limit for the dephasing by a quasimode characterized by its strength Z_T, frequency ω_T, and width γ_0, LP recovers the standard result[13] of a Lorentzian line shape with shift $\Delta\omega_M$ and width full width at half maximum Γ given by

$$\Delta\omega_M=(n+1/2)\lambda\ , \tag{3.1a}$$

$$\Gamma=2n(n+1)\lambda^2/\gamma_0\ , \tag{3.1b}$$

where n is the thermal occupation factor $n=\langle n_T\rangle=(e^{\beta\omega_T}-1)^{-1}$ for the quasimode. LP showed that the coupling constant λ, which has the units of frequency, is given in this model by

$$\lambda=Z_T K_4^{\parallel}/(\mu_\perp\mu_\parallel\omega_M\omega_T)\ , \tag{3.2}$$

where we have changed LP's notation slightly to be consistent with what becomes necessary later in this paper. We denote by λ_0 the value of λ for the specific case of the minimal anharmonicity model, which is obtained by setting $K_4^{\parallel}=-k_M/2(l_0)^2$ in (3.2) and hence yielding (1.8). The force constant k_M can be estimated from $k_M\approx\mu_\perp\omega_M^2$, while the weight Z_T $[0<Z_T<1]$ can be estimated from Eq. (4.34) for the frozen substrate case. Finally, we have in the diatomic adsorbate case,

$$\frac{1}{\mu_\perp}=\frac{1}{M_C+M_O}+\frac{1}{M_S}\ , \tag{3.3}$$

but $\mu_\parallel$ is still given by (2.11). This definitional asymmetry was introduced to reflect the fact that in the single-bond anharmonic model the relative C-O z coordinate is fixed, while the corresponding x coordinate is not. We nevertheless retain the above *definitions* for $\mu_\perp$ and $\mu_\parallel$ from now on, and in particular we still use them in Sec. IV when the internal bond is allowed to flex. The effective mass M_M introduced earlier is for all practical purposes equal to $\mu_\perp$ because, for the reasons discussed in Sec. II A, the renormalization factor Z associated with this mode differs negligibly from unity.

The above results may be specialized to the monatomic adsorbate case by letting $M_O=0$ and $M_C=M_A$ so that $\mu_\perp=\mu_\parallel$ and also letting $Z_T=1$.

The weak-coupling result in (3.1b) is valid as long as $\lambda\ll\gamma_0$. For instance, this weak-coupling result has been used by Dumas, Chabal, and Higashi[3] in the analysis of the temperature dependence of the linewidth for the H-Si stretch mode, and an overall best fit was obtained with $\omega_T=210\ \mathrm{cm}^{-1}$, $\lambda=-5\ \mathrm{cm}^{-1}$, and $\gamma_0=52\ \mathrm{cm}^{-1}$. In this case they attributed the dephasing to a single surface phonon band and λ was found to be close to the value obtained from a Morse form for the central force with appropriate binding parameters. On the other hand, in the case of CO on Pt(111) and Ni(100), the Morse model for the anharmonicity gave typically far too large a value for λ in comparison with observed line shapes, whereas the coupling constant λ_0 gave line shapes in reasonable agreement with experiment. In these situations, the quasimode is the narrow bending resonance (T) in (2.12) and it was necessary to go beyond the weak-coupling limit and use the more general solution for the line shape.

A principal aim of the rest of this paper is to calculate the *effective* value of λ, i.e., λ_{eff}, to use either in (3.1b) if it turns out that $\lambda_{\mathrm{eff}}\ll\gamma_0$ or in the more general theory of LP, Ref. 2, otherwise. In this section we consider the contribution to λ_{eff} due to the inclusion of cubic terms to higher orders. In Sec. IV we, in addition, include the effects on λ_{eff} of allowing the internal bond to flex.

B. Effective vertex

As was first pointed out for this problem by Zhang and Langreth,[9] the cubic terms in (2.14) can have contributions comparable to the x^2z^2 term. In the high-frequency limit, we show that these contributions can usually be regarded as being due to an effective Hamiltonian with a single term, $H_{\mathrm{int}}^{\mathrm{eff}}=\mathcal{K}_4^{\parallel}x^2z^2$. We first show this result in the situation when the frequencies of all parallel modes are well below ω_M, and later generalize to include a possible higher-frequency mode such as the R mode for CO. However, it is not true in the presence of a Fermi resonance.

To find the infrared response and line shape, we calculate the self-energy of the propagator for the AS stretch using the same formalism and notation as LP.[2] Many-body perturbation theory yields seven diagrams[14] contributing to the dephasing to second order in $K_4^{\parallel}$ which are shown in Fig. 3. The four-legged vertices correspond to an interaction involving the first term of H_{int} in (2.14), the three-legged vertices with all solid lines to the second term, and the three-legged vertices with one solid and two dashed lines to the third. As was first pointed out by Zhang and Langreth,[9] two orders of the cubic interactions are equivalent to one order of the quartic interaction. A complete discussion of the many diagrams that can arise is given by Zhang[10] in the context of perpendicular modes.

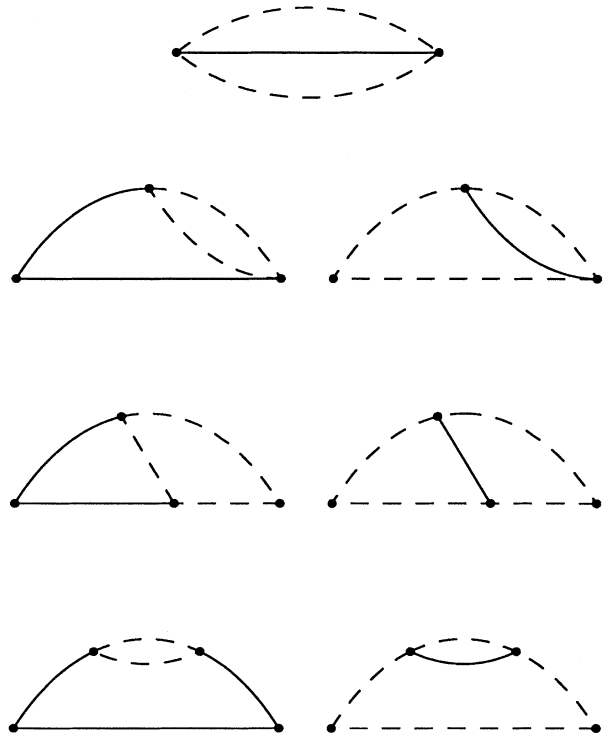

FIG. 3. All second-order (see text) contributions to the linewidth involving both cubic and quartic interactions. The solid lines represent the high-frequency localized mode, while the dashed line represents parallel polarized phonons.

All of these diagrams may be summarized by a single diagram, the first in Fig. 3, with *both* quartic vertices replaced by effective quartic vertices which include pairs of cubic interactions. The resulting effective vertex is shown diagrammatically in Fig. 4, and may be written, using the Matsubara formalism,[15] as

$$\mathcal{K}_4^{\parallel}(i\omega_\nu, ip_\nu, iq_\nu) = K_4^{\parallel} + 3K_3^{\perp}K_3^{\parallel}L_\perp^h(ip_\nu + iq_\nu) + (K_3^{\parallel})^2[L_\parallel^h(i\omega_\nu - ip_\nu) + L_\parallel^h(i\omega_\nu - iq_\nu)] , \tag{3.4}$$

where $L_\perp^h$ and $L_\parallel^h$ are the correlation functions introduced in (2.3) and (2.12) and ω_ν, p_ν, and q_ν are all Matsubara frequencies. The numerical factors are determined by the usual combinatorial factor at each bare vertex (2!2! for $K_4^{\parallel}$, 2!/2 for $K_3^{\parallel}$, and 3! for $K_3^{\perp}$), divided by the number of interchanges of external legs leaving the vertex unchanged [i.e., 4 for (a) and (b), and 2 for (c)].

To continue the argument for an effective vertex to all orders in perturbation theory, one must check that, in the high-frequency limit, all diagrams involving two or more cubic interactions can be rewritten as part of a diagram involving only effective vertices. Figure 5 contains two third-order diagrams which appear very similar. However, in Fig. 5(a), the cubic interactions may be viewed as (b) of the effective vertex of Fig. 4, whereas topology prevents this in Fig. 5(b). Thus, Fig. 5(b) appears to contradict our result. Fortunately, the fact that the two cubic interactions are not joined by a single parallel propagator in 5(b) also means that the corresponding term in the perturbation series contains an extra energy denominator, so that it is of order $O(\omega_T/\omega_M)$ relative to the contribution from 5(a), and may be neglected in the high-frequency limit. This argument applies to all such undesirable diagrams, establishing the regime of validity of the vertex approximation in (3.4) for all coupling strengths.

Now, when we use this vertex in the first diagram of Fig. 3 to evaluate the contribution to the linewidth at the localized mode frequency ω_M to leading order in perturbation theory, we must make the analytic continuation $i\omega_\nu \to \omega_M + i0^+$. The sum of the other Matsubara frequencies picks up contributions from the poles at $\pm\omega_T$. Since ω_T is negligible compared to ω_M in the high-frequency limit, these contributions can be evaluated using the zero-frequency limit of $L_\perp^h$ and the high-frequency limit of $L_\parallel^h$. The zero-frequency limit of $L_\perp^h$ can be obtained directly from (2.3),

$$L_\perp^h(\omega) \to -\frac{1}{2K_2}, \quad \omega \to 0 . \tag{3.5}$$

where we have used the relation in (2.5). We later show that this zero-frequency limit is a general result for a nearest-neighboring central force-constant model for the stretch mode. The high-frequency limit of $L_\parallel^h$ can be obtained from a sum rule for the corresponding spectral function or more directly from the fact that $-L_\parallel^h(\omega)$ is the response of x to an external force F_{ext} acting on the relative x with frequency ω, and that in the limit $\omega \to \infty$, the forces in the x direction between the atoms can be neglected. In this limit the equations of motion for x_1 and x_2 are given by

$$-M_C\omega^2 x_1 = F_{\text{ext}} , \tag{3.6a}$$

$$-M_S\omega^2 x_2 = -F_{\text{ext}} , \tag{3.6b}$$

which immediately yields

$$L_\parallel^h(\omega) \to \frac{1}{\mu_\parallel \omega^2}, \quad \omega \to \infty , \tag{3.7}$$

where $\mu_\parallel$ is given by (2.11). As a corollary one finds from (2.10) that

$$L_\parallel^{h,\text{band}}(\omega) \to \frac{Z_B}{\mu_\parallel \omega^2}, \quad \omega \to \infty , \tag{3.8}$$

where $Z_B = 1 - Z_R$ as always. These two limiting behaviors of $L_\perp^h$ in (3.5) and $L_\parallel^h$ in (3.7) then yield an effective $\mathcal{K}_4^{\parallel}$ of

$$\mathcal{K}_4^{\parallel} = K_4^{\parallel} - 3\frac{K_3K_3^{\parallel}}{2K_2} + 2\frac{(K_3^{\parallel})^2}{\mu_\parallel(\omega_M)^2} . \tag{3.9}$$

Inserting in (2.15c) the definitions of the anharmonic force constants in terms of the anharmonic coefficients of $U(l)$ defined in (2.13) into (3.9), we obtain

$$\mathcal{K}_4^{\parallel} = -\frac{K_2}{l_0^2} + 2\frac{K_2^2}{\mu_\parallel(\omega_M)^2 l_0^2} . \tag{3.10}$$

Hence, $\mathcal{K}_4^{\parallel}$ depends only on the harmonic part of $U(l)$ and the anharmonic part cancels and gives no contribution. This is one of the central results of this paper.

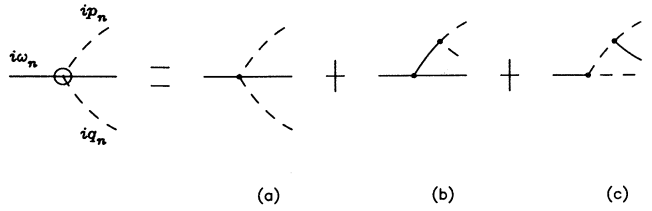

FIG. 4. Renormalized vertex, in terms of which all diagrams of Fig. 3 may be adsorbed into the first one. The solid and dashed lines have the same meaning as in Fig. 3.

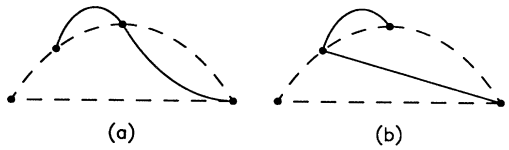

FIG. 5. Two apparently similar third-order (see text) diagrams, but (a) can be included in a third-order diagram involving only effective vertices, whereas (b) cannot. The solid and dashed lines have the same meaning as in Fig. 3.

C. Important special cases

There are two important special cases for which the model considered so far is sufficiently complete that

definitive predictions can be made. These are discussed briefly below. We also give a simple model example which shows directly why the surprising results occur.

1. Dephasing of a monatomic adsorbate

First, we apply this result to a monatomic adsorbate. Using the definition in (3.2) and the relation between K_2 and ω_M implied by (2.5), we can define the effective coupling constant λ_{eff} as

$$\lambda_{\text{eff}}=\lambda_0\left[1-\frac{\mu_\perp}{\mu_\parallel}\right] . \tag{3.11}$$

Comparing this with (1.9) of the Introduction, we see here that $\lambda_{\text{Fermi}}=0$, because there are no Fermi resonances in this case. We consider the stretch mode of an atomic adsorbate such as H on Si. In this case, the frequency of the parallel mode is much less than ω_M, so that the result in (3.11) is directly applicable, which gives $\lambda_{\text{eff}}\approx 0$ since $\mu_\perp=\mu_\parallel$. Thus, we have shown that there is essentially *no* dephasing for a monatomic adsorbate due to the stretching of the principal adsorbate-substrate bond. Small remnant contributions exist due to the fact that ω_M^2/ω_T^2 is not truly infinite, but for practical purposes we have the remarkable result that *neither* the anharmonic nor the harmonic part of the central force gives a contribution to the dephasing linewidth. Thus, in the case of H on Si, for example, where an explanation of the experimental data in terms of a central Morse potential has great appeal, one may well have to look to cubic and quartic anharmonicities in the very small noncentral (bending) forces in order to obtain substantial dephasing.

2. Dephasing of the internal stretch mode of CO

This case is formally identical to the monatomic adsorbate case, because so far as the above results are concerned, C may simply be considered to be part of the substrate and O as a monatomic adsorbate. Because of the high vibrational frequency of the I mode in comparison with all other modes, the results in (2.3), (2.5), and (2.6) can be directly applied to the correlation function for z_0-z_1, but now with the reduced mass $\mu_\perp^{-1}=\mu_I^{-1}\equiv M_{\text{C}}^{-1}+M_{\text{O}}^{-1}$ and $\omega_A^2=k_I/\mu_I$. Similarly, (2.11) becomes $\mu_\parallel^{-1}=M_{\text{O}}^{-1}+M_{\text{C}}^{-1}=\mu_\perp^{-1}$. Therefore the dephasing of the I mode likewise is very small because of the cancellation in (3.11), and again one must look for anharmonicities in the small noncentral bending force. Thus, estimates of the strength of the coupling constant, which we denote λ_{eff}, from experimentally observed linewidths and shifts,[1] should be interpreted with the understanding that the central forces do not contribute.

3. Simple model for cancellation of central force anharmonicity

Why does the central force model produce such a cancellation? For simplicity, consider a single dephasing mode of frequency ω_T in the parallel direction. The harmonic part of the Hamiltonian is then

$$H_{\text{harmonic}}=\frac{p_x^2+p_z^2}{2\mu}+\frac{\mu\omega_M^2 z^2}{2}+\frac{\mu\omega_T^2 x^2}{2} \tag{3.12}$$

and the anharmonic part is correct up to fourth order in the displacements given by (2.14). Now we make a coordinate transformation from Cartesian coordinates to the separation coordinate l and the angle θ between the adsorbate-substrate direction and the perpendicular. In terms of these coordinates, the full Hamiltonian becomes

$$H=\frac{p_l^2}{2\mu}+\frac{p_\theta^2}{2\mu l^2}+\mu\omega_T^2 l^2\sin^2\theta/2+U(l) , \tag{3.13}$$

where p_l and p_θ are conjugate momenta to l and θ. Then, the anharmonic part is given up to fourth order in the displacement $l-l_0$, the angle θ and the momentum p_θ,

$$\begin{aligned}H_{\text{int}}=&K_4^\parallel\left[l_0^2\theta^2-\left[\frac{p_\theta}{\mu\omega_T l_0}\right]^2\right](l-l_0)^2\\&+K_3^\parallel\left[l_0^2\theta^2+3\left[\frac{p_\theta}{\mu\omega_T l_0}\right]^2\right](l-l_0)\\&+K_3^\perp(l-l_0)^3+K_4^\perp(l-l_0)^4 ,\end{aligned} \tag{3.14}$$

where now $K_3^\parallel=\mu\omega_T^2/l_0$, $K_4^\parallel=\mu\omega_T^2/(2l_0^2)$, $K_3^\perp=K_3$, and $K_4^\perp=K_4$. The p_θ terms come from the kinetic term in (3.13), where $(p_\theta)/(\mu\omega_T l_0^2)$ has the same amplitude as θ. In terms of these stretching and bending coordinates the coefficients of the anharmonic terms $K_4^\parallel$ and $K_3^\parallel$ are down by a factor of $(\omega_T/\omega_M)^2$. Thus, in the high-frequency limit (effectively, $\omega_T/\omega_M\to 0$), these terms are negligible, and we are left with a harmonic oscillator with a single high frequency, no longer coupled to a low-frequency mode. Such a system cannot dephase. However, if the potential were not simply central and had some θ dependence, then one could not ignore θ in this limit and it could cause dephasing.

D. Possible Fermi-resonance effects for CO

1. The structure of $L_\perp(\omega)$

As discussed in Sec. I A, one consequence of the cubic anharmonic term $K_3^\parallel x^2 z$ that couples the parallel modes to the stretch mode is that Fermi-resonance effects may appear. Such a resonance is present even in the lowest-order cubic self-energy diagram, and we verify here that it gives to a characteristic satellite to the main line. The infrared line shape is determined from the spectral function of $L_\perp(\omega)$ which is related to the self-energy $S(\omega)$ through a Dyson equation,

$$L_\perp(\omega)=[L_\perp^h(\omega)^{-1}-S(\omega)]^{-1} . \tag{3.15}$$

The lowest-order self-energy diagram S_3 due to the cubic term for $L_\perp$ is shown in Fig. 6 and is given by

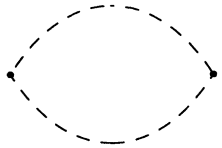

FIG. 6. Lowest-order cubic self-energy diagram.

$$S_3(i\omega_\nu)=-\frac{1}{\beta}\sum_{iq_\nu}2(K_3^{\parallel})^2L_{\parallel}^h(iq_\nu)L_{\parallel}^h(i\omega_\nu-iq_\nu)\ . \tag{3.16}$$

Now, we evaluate the Matsubara sum over iq_ν using the two-pole approximation for $L_{\parallel}^h$ in (2.12) where we have also neglected the width of the quasimode. After doing the analytic continuation $i\omega_\nu\to\omega_M+0^+$, the resonant part for $\omega>0$ of S_3 is given by

$$S_3^{\text{Fermi}}=\frac{\mu_\perp\omega_M\delta\omega_M^2}{2(n+1)}\left[(n+1)\frac{2\omega_+}{\omega^2-\omega_+^2}+n\frac{2\omega_-}{\omega^2-\omega_-^2}\right], \tag{3.17}$$

where $\delta\omega_M$ is given by (1.11) with n_T replaced by its thermal average value n and where $\omega_\pm=\omega_R\pm\omega_T$. In writing (3.17) we have written only those terms that are possibly resonant, and we have assumed no thermal occupation of the R mode. In the case represented in Table I it is the first term in (3.17) that is resonant, so we neglect the second one; we also take $\omega>0$ so that $2\omega_+/(\omega^2-\omega_+^2)\approx(\omega-\omega_+)^{-1}$ neglecting the nonresonant term $(\omega+\omega_+)^{-1}$. Inserting the single-pole approximation for $L_\perp^h(\omega)$ in (2.3) into (3.15) gives

$$L_\perp(\omega)=\frac{1}{2\mu_\perp\omega_M\left[\omega-\omega_M-\dfrac{\delta\omega_M^2}{4(\omega-\omega_R-\omega_T)}\right]}\ . \tag{3.18}$$

This result shows that the stretch mode splits into two modes with frequencies

$$\Omega_M=\omega_M+\Delta\omega_{\text{Fermi}}\ , \tag{3.19a}$$

$$\Omega_{RT}=\omega_R+\omega_T-\Delta\omega_{\text{Fermi}}\ , \tag{3.19b}$$

where $\Delta\omega_{\text{Fermi}}$ is given by (1.10). In the limit of weak coupling $\delta\omega_M\ll|\omega_M-\omega_R-\omega_T|$, the quantity $\Delta\omega_{\text{Fermi}}$ vanishes, which implies that the mode at Ω_M derives from the M or stretch mode, while the mode at Ω_{RT} derives from a combination of the modes R and T. The relative weight W_{RT}/W_M of these two modes is given by

$$\frac{W_{RT}}{W_M}=\frac{\left[1+\left[\dfrac{\delta\omega_M}{\omega_M-\omega_R-\omega_T}\right]^2\right]^{1/2}-1}{\left[1+\left[\dfrac{\delta\omega_M}{\omega_M-\omega_R-\omega_T}\right]^2\right]^{1/2}+1}\ , \tag{3.20}$$

where here the radical sign implies the positive square root.

If we take the values of the parameters from Table I then one obtains the following values (in cm^{-1}) for $\delta\omega_M$ and $\omega_M-\omega_R-\omega_T$ at $T=0$:

	Pt(111)	Cu(100)	Ni(100)	Ir(100)
$\delta\omega_M$	26	28	42	28
$\omega_M-\omega_R-\omega_T$	1	23	69	19

These were the values used to calculate the bare strength ratios W_{RT}/W_M that appear in the Introduction, which were in conflict with experiment. Technically, one should use the measured value of the M mode for Ω_M rather than ω_M, and if there were any hope to use such a procedure to remedy the conflict with experiment we would have been more careful. However, for example, for the Pt(111) case if one took $\Omega_M-\omega_R-\omega_T$ to be 1 cm^{-1} as on the first line above, then it is clearly smaller than the theoretical minimum for this quantity ($\frac{1}{2}\delta\omega_M$) even at $T=0$ and the conflict just shows up in another way.

2. *Renormalized coupling constant* λ_{eff}

In the case of the M mode of the adsorbed CO molecule, ω_R is comparable to ω_M and we can no longer use the high-frequency limit of $L_{\parallel}^h$ in (3.7). Therefore we evaluate the effective vertex in (3.4) for CO using an appropriate $L_{\parallel}^h$ for the parallel motion. Nevertheless, we can still use the static limit for $L_\perp^h$ in (3.5), because we still have $\omega_M\gg\omega_T$. This means that the cancellation of the cubic and quartic terms in the bond stretching still cancel exactly [arising from the first two terms in (3.9)], which implies that the minimal anharmonicity model and the Morse potential model are identical. This is satisfying because LP showed for CO/Pt(111) that the minimal anharmonicity model gave linewidths of the right order of magnitude to be consistent with experiment, while the "more realistic" Morse model gave linewidths that were more than an order of magnitude too large (before consideration of the above cancellation from the cubic terms, which was then not known). However, as discussed in Sec. I C 1, the cubic terms that cause this cancellation themselves give rise to additional predictions in this single-bond model which are not observed experimentally.

In evaluating the contribution of $L_{\parallel}^h$ to the effective vertex (3.4) we use (2.10). As mentioned earlier, we cannot take the infinite frequency limit in the second term, because ω is comparable to ω_R. However the first term $L_{\parallel}^{h,\text{band}}(\omega)$ can be replaced by its high-frequency limit (3.8) because $\omega\gg\omega_{\max}$. We therefore obtain

$$\lambda_{\text{eff}}=\lambda_0\left[1-Z_B\frac{\mu_\perp}{\mu_{\parallel}}\right]+\lambda_{\text{Fermi}}\ . \tag{3.21}$$

The quantity λ_{Fermi} comes from the contribution of the last term of (2.10) to (3.4), which is

$$\frac{(K_{\parallel})^2}{2\omega_T\mu_{\parallel}}\left[\frac{2\omega_+}{\omega^2-\omega_+^2}+\frac{2\omega_-}{\omega^2-\omega_-^2}\right]\ . \tag{3.22}$$

There are several cases to consider. The first is

$$|\omega_M-\omega_\pm|\gg\delta\omega_M\ . \tag{3.23}$$

Then, one is only marginally close to a Fermi resonance and the various frequency and spectral weight renormalizations discussed in Sec. III D 1 are unimportant. Then, one may set $\omega=\omega_M$, and one finds that

$$\lambda_{\text{Fermi}}=-\lambda_0\frac{Z_R\mu_\perp\omega_M^2}{4\mu_{\parallel}\omega_R}\left[\frac{2\omega_+}{\omega_M^2-\omega_+^2}+\frac{2\omega_-}{\omega_M^2-\omega_-^2}\right]\ . \tag{3.24}$$

Thus, one obtains an effective coupling constant which can be greatly enhanced by the presence of the nearly resonant denominators. The arguments that lead to it can be rigorously checked by evaluating the diagrams for finite ω_M, and then taking the high-frequency limit. Furthermore, the classical limit (which contains diagrams to all orders) also exhibits exactly the same effective coupling constant, and obeys the same criterion for breakdown of the vertex approximation.[16]

We note here several regimes for λ_{Fermi} in (3.24). In the limit $\omega_R \ll \omega_M$, $\lambda_{\text{Fermi}} \approx -\lambda_0 Z_R \mu_\perp / \mu_\parallel$ and λ_{eff} reduces as it should to the result in (3.11). Equation (3.21) also exhibits the correct limit for a monatomic adsorbate, where $Z_R = 0$, $Z_B = 1 - Z_R = 1$, hence yielding (3.11), which in this case gives zero because $\mu_\parallel = \mu_\perp$. In the intermediate regime, however, λ_{Fermi} can attain much larger absolute values than λ_0 due to the denominators, which brings us to the second case discussed below.

Next we consider the case where the condition (3.23) fails because one is too close to the resonance at ω_+. Then the first term in (3.22) dominates and other contributions can be neglected. However, the Fermi-resonance renormalizations must be included. If one wants to calculate the dephasing for the resonance at Ω_M, then the relevant term in (3.22) is (i) to be evaluated at $\omega = \Omega_M$ instead of $\omega = \omega_M$, and (ii) it is to be multiplied by W_M as defined by (3.20), where $W_M + W_{RT} = 1$. The latter correction occurs because the vertex connects two $L_\perp$ correlation functions for which the resonance at Ω_M has the weight W_M; each such correlation function contributes a factor of $\sqrt{W_M}$ to the effective vertex. The overall result of these corrections is to give a λ_{Fermi} equal to that of (1.12). The warnings about the validity below (1.12) apply to this derivation as well, because it is hard to see how this argument could be extended beyond second-order perturbation theory. The third case, where the condition (3.23) fails because one is too close to the resonance at ω_-, is equally easy to discuss, but we do not give the details because it does not seem relevant to the materials for which we have experimental data.

For the materials in Table I the values for $\delta\omega_M$ and $\omega_M - \omega_R - \omega_T$ given above indicate that it is the second case that is most relevant. Using these data we calculate the following values for λ_{eff}. Values of λ_0 are also included.

	Pt(111)	Cu(100)	Ni(100)	Ir(100)
λ_{eff}	169	7.5	8.3	11
λ_0	−0.73	−1.07	−1.66	−0.77

As one can see, the values produced by this theory are preposterous and would lead to linewidths too large by orders of magnitude. That the theory that produced them would breakdown for values this large is not the greatest of our problems.

IV. DEPHASING AND FERMI-RESONANCE EFFECTS IN THE DOUBLE-BOND ANHARMONIC MODEL

In the case of the AS stretch mode of the CO molecule we found strong resonance effects in the single-bond anharmonic model arising from the cubic term $K^{\parallel}_{3} x^2 z$ in (2.14). We show here that the single-bond anharmonic model is incomplete for the M stretch mode due to the presence of a stretch mode I of higher frequency, which makes it necessary to introduce the anharmonicity from the central force of the internal bond of the CO molecule.

A. Double-bond anharmonic model

The inclusion of the anharmonicity from the central force associated with the internal stretch is straightforward. The total potential energy associated with the stretching of the two bonds is given by the sum $U_M(l_M) + U_I(l_I)$ of the potential energies of the C-S bond and the C-O bond (they are hereafter referred to as M and I, respectively) where l_M and l_I are the corresponding bond distances. We make the same kind of expansion of U_M and U_I around their potential minima at $l_M = l_{0M}$ and $l_I = l_{0I}$, respectively, as done in the single-bond case in (2.13),

$$\begin{aligned} U_M(l_M) + U_I(l_I) = {} & K_{2,M}(l_M - l_{0M})^2 \\ & + K_{3,M}(l_M - l_{0M})^3 + K_{4,M}(l_M - l_{0M})^4 \\ & + K_{2,I}(l_I - l_{0I})^2 + K_{3,I}(l_I - l_{0I})^3 \\ & + K_{4,I}(l_I - l_{0I})^4 , \end{aligned} \tag{4.1}$$

where the contributions from the different bonds are distinguished by introducing the subscripts M and I. The anharmonic part H_{int} is then obtained by expanding $l_M - l_{0M}$ and $l_I - l_{0I}$ in their parallel and perpendicular coordinates $\tilde{x}_i$ and $\tilde{z}_i$, respectively, as given in terms of the atomic coordinates by

$$\begin{aligned} & \tilde{x}_1 = x_1 - x_2, \quad \tilde{x}_2 = x_0 - x_1 , \\ & \tilde{z}_1 = z_1 - z_2, \quad \tilde{z}_2 = z_0 - z_1 , \end{aligned} \tag{4.2}$$

and keeping terms in the potential energy up to fourth order in these coordinates,

$$\begin{aligned} H_{\text{int}} = {} & K^{\parallel}_{3,M} \tilde{x}_1^2 \tilde{z}_1 + K^{\parallel}_{3,I} \tilde{x}_2^2 \tilde{z}_2 + K^{\parallel}_{4,M} \tilde{x}_1^2 \tilde{z}_1^2 + K^{\parallel}_{4,I} \tilde{x}_2^2 \tilde{z}_2^2 \\ & + K^{\parallel}_{3,M} \tilde{z}_1^3 + K^{\parallel}_{3,I} \tilde{z}_2^3 + K^{\parallel}_{3,M} \tilde{z}_1^4 + K^{\parallel}_{3,I} \tilde{z}_2^4 . \end{aligned} \tag{4.3}$$

The anharmonic force constants $K^{\parallel}_{3,M,I}$, $K^{\parallel}_{4,M,I}$, $K^{\parallel}_{3,M,I}$, and $K^{\parallel}_{4,M,I}$ are determined from the expansion coefficients of the central potentials in the same manner as in (2.14) for the single-bond case. Note that the magnitude of the anharmonic force constants in (4.3) are set by the stretching force constants $k_M \equiv 2K_{2,M}$ and $k_I \equiv 2K_{2,I}$.

The larger anharmonicity of the bond I by a factor about k_I / k_M is reduced in the case of the dephasing of the mode M. This arises because the high frequency of the I mode compared to the frequency of the M mode gives a much smaller stretching $\tilde{z}_2$ of the bond I than the stretching $\tilde{z}_1$ of the M bond. Earlier, we let $\tilde{z}_2 = 0$, an assumption which reduces the double-bond anharmonic model in (4.1) to the single-bond anharmonic model in (2.13). This assumption is invalid, however, and we will show later that to leading order in k_M / k_I,

$$\frac{\tilde{z}_2}{\tilde{z}_1}=\frac{M_O k_M}{(M_O+M_C)k_I} . \tag{4.4}$$

Although this ratio is small, it is not sufficiently small to overcome that fact that the internal stretch has a much larger force constant, and it is the force constant *times* the displacement to a power determined by which term one is considering in (4.3) which is the important quantity in discussing anharmonic effects. Hence, anharmonic terms due to U_I with single powers of $\tilde{z}_2$ do give a contribution to the anharmonicity in this limit. The only term in (4.3) with this property is the cubic term $K^{\parallel}_{3,I}\tilde{x}_2^2\tilde{z}_2$ and we will show later that this is the only relevant anharmonic term introduced by U_I for the dephasing in the limit $k_I/k_M \to \infty$.

B. Correlation functions in the harmonic approximation

Before generalizing the diagrammatic expansion to the double-bond anharmonic model, we need to introduce the necessary correlation functions for the perpendicular and parallel displacements of the molecule. We give analytical expressions for these functions in the frozen substrate situation when taking the appropriate limit of widely separated adsorbate-mode frequencies. The effects of coupling the adsorbate modes to the substrate modes are calculated numerically for CC on Pt(111) using adsorbate lattice-dynamical techniques.

1. General considerations and sum rules

The particular form of $H_{\rm int}$ in (4.3) shows that we need matrices of correlation functions $\tilde{L}^h_{\perp,kl}$ and $\tilde{L}^h_{\parallel,mn}$ for the parallel and perpendicular displacements, respectively, when evaluating the diagrammatic expansion of the self-energy. As shown in LP, these matrices can be expressed, using the normal modes of the adsorbate-substrate system, as

$$\tilde{L}^h_{\sigma,kl}(\omega)=\sum_{i,j}\frac{f_{ki}R_{\sigma,ij}(\omega)f_{lj}}{\sqrt{M_i M_j}} , \tag{4.5}$$

where the collective indices i,j each label both an atom and a Cartesian direction in space and R_σ is a resolvent matrix to the dynamical matrix D_σ for the displacements belonging to the same symmetry classes as for the perpendicular $\sigma=\perp$ and parallel adsorbate modes $\sigma=\parallel$, respectively. The resolvent R_σ of a dynamical matrix D_σ is defined in the usual way as

$$R_{\sigma,ij}(\omega)=[(\omega^2 I-D_\sigma)^{-1}]_{ij} . \tag{4.6}$$

The expansions coefficients f_{ki} relate the bond coordinates to the atomic coordinates and are simply defined as

$$\tilde{z}_k=\sum_i f_{ki}z_i , \tag{4.7a}$$

$$\tilde{x}_m=\sum_i f_{mi}x_i , \tag{4.7b}$$

where the index i now runs only over the O, C, and the nearest-neighboring substrate atom. These coefficients are given directly by the relations in (4.2) and are summarized below in matrix form:

$$\mathbf{f}=\begin{matrix}&\begin{matrix}0&1&2\end{matrix}\\ \begin{matrix}1\\2\end{matrix}&\begin{bmatrix}0&1&-1\\1&-1&0\end{bmatrix}\end{matrix} , \tag{4.8}$$

where the numbers on the top border represent the values of i corresponding to the atomic coordinates, while the numbers on the left border represent the values of k corresponding to the bond coordinates. The relationship between the various coordinates labeled by these subscripts is illustrated in the mnemonic below:

	O		C		S
ij	0		1		2
$klmn$		$\leftarrow\tilde{2}\rightarrow$		$\leftarrow\tilde{1}\rightarrow$	

In addition, in Table II we summarize the subscripts used in this section.

In the frozen substrate situation, we have two perpendicular and parallel modes, respectively, and the resolvents in (4.6) for $\sigma=\perp$ and $\parallel$ are given as a sum over two simple poles,

$$R_{\sigma,ij}(\omega)=\sum_\lambda\frac{e^{(\infty)}_{\lambda,i}e^{(\infty)}_{\lambda,j}}{[\omega^2-(\omega^{(\infty)}_\lambda)^2]} , \tag{4.9}$$

where $\lambda=M,I$ and $\lambda=T,R$ for $\sigma=\perp$ and $\parallel$, respectively. The normal modes λ have the normalized mass-weighted displacement fields

$$e^{(\infty)}_{\lambda,i}\propto\sqrt{M_i}x_i \quad \text{for } \lambda=T,R , \tag{4.10a}$$

$$e^{(\infty)}_{\lambda,i}\propto\sqrt{M_i}z_i \quad \text{for } \lambda=M,I , \tag{4.10b}$$

and frequencies $\omega^{(\infty)}_\lambda$. They are the eigenvectors and eigenvalues of the dynamical matrix in the rigid substrate situation, defined by

$$\sum_j D^{(\infty)}_{\sigma,ij}e^{(\infty)}_{\lambda,j}=(\omega^{(\infty)}_\lambda)^2 e^{(\infty)}_{\lambda,i} . \tag{4.11}$$

As already stressed in Sec. II, the vibrational frequencies for the M, I, and R modes are well above $\omega_{\rm max}$. They experience an upward shift when coupled to the substrate modes, and therefore remain above the phonon continuum. The relation between the correlation functions and the resolvent in (4.5) shows directly that the correlation functions are given by a sum over the substrate phonon band contribution and the localized adsorbate modes as

$$\tilde{L}^h_{\sigma,kl}(\omega)=\tilde{L}^{h,\rm band}_{\sigma,kl}(\omega)+\sum_{\text{localized}\lambda}C_{\lambda,k}C_{\lambda,l}L^h_\lambda(\omega) , \tag{4.12}$$

TABLE II. Summary of subscript and superscript indices used in Sec. IV. The final column indicates whether the Einstein summation convention is implied on repeated indices.

Symbol	Meaning	Values	Summation
σ	which symmetry	$\perp,\parallel$	no
λ	which mode or pole	M,I,T,R	no
$klmn$	which bond	1,2	yes
ij	which atom	0,1,2	no

where

$$L^h_\lambda(\omega)=\frac{Z_\lambda}{\mu_\parallel(\omega^2-\omega^2_\lambda)} , \tag{4.13}$$

and $\mu_\parallel$ is given as before by (2.11). By *localized* λ in (4.12) we mean those modes with frequencies lying outside the phonon band, that is $\lambda=M,I$ for $\sigma=\perp$ and $\lambda=R$ for $\sigma=\parallel$; in an exact treatment the T mode is a resonance in $\tilde{L}^{h,\text{band}}_{\sigma,kl}(\omega)$ as further clarified below; for the frozen lattice approximation to adsorbate motion, however, it is most convenient to take $\tilde{L}^{h,\text{band}}_{\sigma,kl}(\omega)=0$ and include the T mode in the sum over localized λ. Here we anticipate a convenient representation for the treatment of the dephasing of the mode M by having the same mass $\mu_\parallel$ for all L^h_λ and also by choosing the normalization

$$C_{\lambda,1}=1 . \tag{4.14}$$

The spectral strengths Z_λ in (4.13) can then be shown from (4.5), (4.9), (4.19), and (4.14) to be given in terms of the normalized mass-weighted displacement fields $e_{\lambda,i}$ by

$$Z_\lambda=\left[\sum_i f_{1i}\left[\frac{\mu_\parallel}{M_i}\right]^{1/2}e_{\lambda,i}\right]^2 \tag{4.15}$$

and the expansion coefficients $C_{\lambda,2}$ defined in (4.19),

$$C_{\lambda,2}=\frac{\sum_i f_{2i}M_i^{-(1/2)}e_{\lambda,i}}{\sum_i f_{1i}M_i^{-(1/2)}e_{\lambda,i}} . \tag{4.16}$$

In the frozen substrate situation we have according to (4.7b) and (4.10b) that these $C_{\lambda,2}$'s are just displacement ratios of the bond coordinates

$$C^{(\infty)}_{\lambda,2}=\left.\frac{\tilde{z}_2}{\tilde{z}_1}\right|_{\omega=\omega^{(\infty)}_\lambda} \text{ for } \lambda=M,I \tag{4.17a}$$

$$C^{(\infty)}_{\lambda,2}=\left.\frac{\tilde{x}_2}{\tilde{x}_1}\right|_{\omega=\omega^{(\infty)}_\lambda} \text{ for } \lambda=T,R . \tag{4.17b}$$

Later, we will calculate Z_λ and $C_{\lambda,2}$ in the full lattice-dynamical situation by calculating numerically the residues of $\tilde{L}^h_{\sigma,11}$ and $\tilde{L}^h_{\sigma,21}$ at $\omega=\omega_\lambda$ by a continued fraction technique for the resolvent.[11]

The remaining parallel adsorbate mode T overlaps with the substrate phonon band and broadens into a narrow resonance which is not a well-defined normal mode with a localized displacement field. Such a resonance is characterized by the dynamical matrix having a complex eigenvalue $(\omega_T-i\gamma_0/2)^2$ close to the real axis, with a non-normalizable eigenmode. This gives rise to a pole in the correlation functions on the unphysical sheet of the Riemann surface. In deriving the generalized vertex approximation, we use only the single pole in the band contribution to the external legs while we use only the high-frequency limit for the band contribution to the internal legs. We find the matrix of residues for this single pole as can be seen from Table III to be well approximated by a factorizable form,

$$C_{T,k}C_{T,l}L^h_T(\omega) , \tag{4.18}$$

TABLE III. Pole and band parameters in the correlation functions for the parallel adsorbate modes of CO on Pt(111). The band weights of the correlation functions $L^h_{\parallel,kl}(\omega)$ are given by the integrals $(\mu_\parallel/\pi)\int_{\text{band}} d\omega\,\omega\bar{l}_{\parallel,kl}(\omega)$, and the residues by $2\omega\mu_\parallel[(d/d\omega)(L^h_{\parallel,kl})^{-1}]^{-1}$, γ_0 is the width of the resonance mode T and is calculated as $\gamma_0=2(L^h_{\parallel,kl})^{-1}[(d/d\omega)(L^h_{\parallel,kl})^{-1}]^{-1}$.

	$L^h_{\parallel,11}$	$L^h_{\parallel,12}$	$L^h_{\parallel,22}$
Band weight	0.229	−0.117	0.061
T residue	0.216	−0.112	0.0585
γ_0 (cm^{-1})	1.9	1.9	1.9
R residue	0.771	0.851	0.939

where we have the same normalization of $C_{T,1}$ as in (4.14) and $L^h_T(\omega)$ is defined as in (4.13), but now with a pole at $\omega_T-i\gamma_0/2$. This single pole is the only contribution to $\tilde{L}^{h,\text{band}}_{\sigma,kl}(\omega)$ in the frozen substrate situation where the resonance turns into a true localized state and the parameters $C_{T,1}$ and Z_T can then be calculated as in (4.15) and (4.16). While in the full lattice-dynamical calculation these quantities were calculated numerically from the residues of $\tilde{L}^h_{\parallel,11}$ and $\tilde{L}^h_{\parallel,21}$ at $\omega=\omega_T$ by a continued fraction technique for the resolvent.[11] In this latter situation we will later see that this single pole in (4.18) dominates the band contribution to $\tilde{L}^{h,\text{band}}_{\sigma,kl}(\omega)$.

In the case of the perpendicular modes we find to a very good approximation that we can neglect the band contribution, so that in the both cases we arrive at a two-pole approximation for the correlation function,

$$\tilde{L}^h_{\sigma,kl}(\omega)=\sum_\lambda C_{\lambda,k}C_{\lambda,l}L^h_\lambda(\omega) . \tag{4.19}$$

In particular, $\tilde{L}^h_{\parallel,11}=L^h_R+L^h_T$ has the same form as in (2.12) with the same definition of the spectral strengths $Z_{R,T}$. The quality of the two-pole approximation can be checked by the sum rule

$$\int\frac{d\omega}{2\pi}2\omega\bar{l}^h_{\sigma,kl}(\omega)=\sum_i\frac{f_{ki}f_{li}}{M_i} \tag{4.20}$$

which may easily be derived from Eq. (35) in LP. The quantity $\bar{l}^h_{\sigma,kl}$ is the spectral function of $\tilde{L}^h_{\sigma,kl}$,

$$\bar{l}^h_{\sigma,kl}(\omega)=-2\,\text{Im}\tilde{L}^h_{\sigma,kl}(\omega+i0^+) . \tag{4.21}$$

Applying this sum rule to (4.19) for $k=l=1$ gives for the parallel and perpendicular modes separately,

$$\sum_\lambda Z_\lambda=1 . \tag{4.22}$$

For the general case the sum should include the contribution from the band. In particular for the parallel modes, the contribution from the T mode is included in the band contribution.

2. ⊥ *modes*

We now turn to the calculation of the $C_{M,2}$ and the zero-frequency limit of $\tilde{L}^h_{\perp,k1}(\omega)$ which are needed to cal-

culate the dephasing of the mode M. This can be done readily in the frozen substrate situation in the limit $k_I/k_S \to \infty$ using the equation of motion for $\tilde{L}^h_{\perp,kl}$ rather than diagonalizing the dynamical matrix. From the definition of $\tilde{L}^h_{\perp,kl}$ in (4.5), it follows that $-\tilde{L}^h_{\perp,k1}(\omega)$ gives the response of the coordinate $\tilde{z}_k$ to an external force F_{ext} with frequency ω acting on the coordinate $\tilde{z}_1$. In the rigid substrate situation $z_2=0$, the equations of motion for the atomic coordinates in the presence of this external force are given by

$$-M_O\omega^2 z_0 = -k_I(z_0-z_1) , \tag{4.23a}$$

$$-M_O\omega^2 z_1 = -k_I(z_1-z_0)-k_M z_1+F_{\text{ext}} . \tag{4.23b}$$

The equation of motion for the C atom and the coordinate transformation in (4.2) then gives directly

$$\frac{\tilde{z}_2}{\tilde{z}_1} = \frac{M_O\omega^2}{k_I - M_O\omega^2} . \tag{4.24}$$

Now, we can eliminate k_I from (4.23b) and inserting the relation between $\tilde{z}_2$ and $\tilde{z}_1$ into (4.24) which gives the response of $\tilde{z}_1$ to F_{ext} as,

$$\tilde{z}_1 = \frac{F_{\text{ext}}}{k_M-(M_C+M_O)\omega^2-\dfrac{(M_O\omega^2)^2}{k_I-M_O\omega^2}} . \tag{4.25}$$

This expression gives then directly $\tilde{L}^h_{\perp,11}(\omega)$ and to leading order in k_M/k_I,

$$\tilde{L}^h_{\perp,11}(\omega) = \frac{1}{(M_C+M_O)(\omega^2-\omega_M^2)} + \frac{M_O}{M_C(M_O+M_C)(\omega^2-\omega_I^2)} , \tag{4.26}$$

where in this limit $\omega_M^2 = k_M/(M_C+M_O)$ and $\omega_I^2 = k_I/\mu_I$. Now, using Eq. (4.17b), we obtain directly from (4.24)

$$C_{M,2} = \frac{M_O k_M}{(M_C+M_O)k_I} , \tag{4.27a}$$

$$C_{I,2} = -\left[1+\frac{M_C}{M_O}\right] . \tag{4.27b}$$

This result also proves the relation between $\tilde{z}_2$ and $\tilde{z}_1$ in (4.4) in this limit. In Table IV, we have compared the result for $C_{M,2}$ in (4.27b) with the result from the full lattice-dynamics calculation.

The zero frequency of $\tilde{L}^h_{\perp,k1}(\omega)$ can be evaluated directly in the full lattice-dynamical calculation without making any restrictions such as having a rigid substrate or taking the limit $k_M/k_I \to 0$. This is because $-\tilde{L}^h_{\perp,k1}(\omega=0)=\tilde{z}_i$ is the response of $\tilde{z}_k$ to an external static force F_{ext} applied to the coordinate $\tilde{z}_1$. The equilibrium conditions in the presence of F_{ext} for the coordinates z_i of the atoms $i=0,1$ are in the nearest-neighboring force-constant model given by

$$0 = -k_I(z_0-z_1) , \tag{4.28a}$$

$$0 = -k_I(z_1-z_0)-k_M(z_1-z_2)+F_{\text{ext}} . \tag{4.28b}$$

These conditions give right away that $\tilde{z}_2=0$ and $\tilde{z}_1=F_{\text{ext}}/k_M$, which proves directly the general result

$$\tilde{L}^h_{\perp,k1}(\omega=0) = -\frac{\delta_{k1}}{k_M} . \tag{4.29}$$

This zero-frequency result can then simply be understood from the fact that the response of the bond M to an applied static force is not influenced by its environment.

Finally, we note from the fact that the calculated spectral strengths for the two adsorbate modes exhaust the spectral sum rule to a very good approximation which justifies our neglect of the band contribution.

3. $\parallel$ modes

Now, we turn to the evaluation of the coefficients $C_{\lambda,2}$ and Z_λ for the adsorbate modes R and T and the high-frequency limit of $\tilde{L}^{h,\text{band}}_{\parallel,kl}$. In the frozen substrate situation, we do the evaluation of these coefficients by directly diagonalizing the (2×2)-dynamical matrix in the limit $\omega_T \ll \omega_R$ and use the results in (4.15) and (4.16). The resulting normal mode frequencies are given by

$$(\omega_R^{(\infty)})^2 = \left[1+\frac{M_O}{M_C}\left[1+\frac{l_{0I}}{l_{0M}}\right]^2\right]\frac{B_R}{l_{0I}^2 M_O} , \tag{4.30a}$$

$$(\omega_T^{(\infty)})^2 = \frac{1}{\left[1+\dfrac{M_O}{M_C}\left[1+\dfrac{l_{0I}}{l_{0M}}\right]^2\right]}\frac{B_T}{l_{0M}^2 M_C} , \tag{4.30b}$$

with mass-weighted displacement fields,

TABLE IV. Coefficients, spectral strengths and renormalization parameters for CO on Pt(111). The label α denotes either the continuum band of phonons B, or an adsorbate mode T, R, M, or I.

$\alpha=$	B	T	R	M	I
Z_α	0.229	0.216	0.771	0.404	0.596
$Z_\alpha^{(\infty)}$		0.234	0.766	0.429	0.571
$C_{\alpha,2}$		0.665	−1.417	0.117	−1.66
$C_{\alpha,2}^{(\infty)}$		0.566	−1.479	0.111	−1.75
$g_{\alpha,T}$	2.15	2.16	2×10^{-6}		
$g_{\alpha,T}^{(\infty)}$		1.75	0.024		

$$\frac{e^{(\infty)}_{R,0}}{e^{(\infty)}_{R,1}} = -\left[\frac{M_C}{M_O}\right]^{1/2}\frac{l_{0M}}{l_{0I}+l_{0M}}, \tag{4.31a}$$

$$\frac{e^{(\infty)}_{T,0}}{e^{(\infty)}_{T,1}} = \left[\frac{M_O}{M_C}\right]^{1/2}\frac{l_{0I}+l_{0M}}{l_{0M}} . \tag{4.31b}$$

Note that the displacement field $e^{(\infty)}_{T,i}/\sqrt{M_i}$ associated with the mode T is a pure rotation around the substrate atom. The coefficients $C_{\lambda,2}$ can now be obtained from (4.31b) by use of (4.10b) and (4.7b) to obtain the bond amplitude ratios for use in (4.17b). One finds

$$C^{(\infty)}_{R,2} = -\left[1+\frac{M_C}{M_O}\frac{l_{0M}}{l_{0M}+l_{01}}\right], \tag{4.32a}$$

$$C^{(\infty)}_{T,2} = \frac{l_{0I}}{l_{0M}} . \tag{4.32b}$$

Then, the spectral strength of the mode T may be obtained, for example, from (4.15) as

$$Z^{(\infty)}_T = \frac{1}{1+\frac{M_O}{M_C}\left[1+\frac{l_{0I}}{l_{0M}}\right]^2} . \tag{4.33}$$

These results for $C_{\lambda,2}$ and Z_T are compared with the results obtained numerically in full lattice-dynamics calculation in Table IV.

The high-frequency limit of $\tilde{L}^{h,\text{band}}_{\parallel,kl}$ is dominated by the term ω^{-2} and can be expressed as

$$\tilde{L}^{h,\text{band}}_{\parallel,kl}(\omega) = \frac{Z_B B_{\parallel,kl}}{\mu_\parallel \omega^2}, \quad \omega\to\infty . \tag{4.34}$$

Here, we anticipated a form that conforms with (4.13) and (4.19) and Z_B is determined from the normalization $B_{\parallel,11}=1$. For instance, if keeping only the single-pole contribution (4.18) in the band and neglecting the band contribution, $Z_B=Z_T$ and $B_{\parallel,kl}=C_{T,k}C_{T,l}$. Now, in the full lattice-dynamical calculation, Z_B and $B_{\parallel,kl}$ can be determined from the observation that the coefficient of ω^{-2} of the high-frequency limit of $\tilde{L}^h_{\parallel,kl}(\omega)$ is given by the moment $\sum_i (f_{ki}f_{li})/(M_i)$ in the sum rule (4.20) and the corresponding limit of the pole from the localized mode (R) in (4.12) as

$$Z_B = 1 - Z_R , \tag{4.35a}$$

$$Z_B B_{\parallel,21} = -\frac{\mu_\parallel}{M_C} - Z_R C_{R,2} , \tag{4.35b}$$

$$Z_B B_{\parallel,22} = \frac{\mu_\parallel}{\mu_I} - Z_R C^2_{R,2} . \tag{4.35c}$$

Note that the calculated single-pole strength Z_T accounts almost for all strength Z_B in the band, $Z_T/Z_B \approx 0.94$ for CO on Pt(111).

4. Application to the effective charge

The infrared line shape is determined from the spectral function of the correlation function for a dipole active displacement field u^*. In this case, u^* has contributions from both bonds,

$$u^* = \sum_k e^*_k \tilde{z}_k , \tag{4.36}$$

where e^*_k are the corresponding effective charges. This shows that we need to consider $\tilde{L}_{\perp,kl}$, Eq. (4.19). Now, we are primarily interested in the mode M and near the corresponding resonance frequency, $\tilde{L}^h_{\perp,kl}$ in (4.13) is dominated by a single pole. Therefore for $\omega\approx\omega_M$ the sum over λ in (4.19) collapses, leaving

$$\tilde{L}_{\perp,kl}(\omega) = C_{M,k}C_{M,l}L_M(\omega) . \tag{4.37}$$

Then, using (4.36) to construct the dipole-dipole correlation function, one finds using (4.14) that it is

$$(e^*_M)^2 L_M(\omega) , \tag{4.38}$$

where

$$e^*_M = e^*_1 + C_{M,2}e^*_2 . \tag{4.39}$$

This implies that the effective charge for the mode M has a contribution from the internal bond. For instance, in the case of CO on Pt(111) this contribution can be most important. The measured effective charge for the mode M, $|e^*_M|=0.17e$ is much smaller than the measured effective charge $|e^*_I|=1.5e$ for the mode I where $e^*_I = e^*_2 + e^*_1/C_{I,2}$.[17] This gives two possible values for the contribution of the internal bond stretch to the dipole activity of M, relative to that of the adsorbate-substrate stretch, i.e., $C_{M,2}e^*_2/e^*_1 \approx 3$ and -0.5. In particular, for the in-phase alternative, the internal bond stretch dominates this dipole activity.

C. Cubic anharmonicity and Fermi-resonance effects

Here we first consider the effect of the lowest-order cubic self-energy diagram on the line shape. The self-energy S_{kl} of the $\tilde{L}_{\perp,kl}$ is defined from the matrix Dyson equation as

$$\tilde{L}_{\perp,kl} = \tilde{L}^h_{\perp,kl} + \tilde{L}^h_{\perp,kk'}S_{k'l'}\tilde{L}_{\perp,l'l} , \tag{4.40}$$

where the summation over repeated bond indices is implied. Again, we are interested in the case $\omega\approx\omega_M$ so that the single-pole expression (4.37) suffices. Inserting it into (4.40) gives a scalar Dyson equation

$$L_M(\omega) = L^h_M(\omega) + L^h_M(\omega)S_M(\omega)L_M(\omega) \tag{4.41}$$

with a self-energy

$$S_M = C_{M,k}C_{M,l}S_{kl} . \tag{4.42}$$

Now, we turn to the evaluation of the lowest-order cubic self-energy diagram in the double-bond anharmonic model. First, we have to give an expression for the vertex for the cubic interaction between the perpendicular and parallel modes in this model. This cubic interaction couples three L's in the combination $\tilde{K}^{\parallel}_{3,klm}\tilde{L}^h_{\perp,kk'}\tilde{L}^h_{\parallel,l'l}\tilde{L}^h_{\parallel mm'}$, where

$$\tilde{K}^{\parallel}_{3,klm} = K^{\parallel}_{3,M}\delta_{k1}\delta_{l1}\delta_{m1} + K^{\parallel}_{3,I}\delta_{k2}\delta_{l2}\delta_{m2} . \tag{4.43}$$

The lowest-order cubic self-energy diagram in Fig. 6 is built up by two such vertices and is given by

$$S^{(3)}_{kl}(i\omega_\nu)=-\frac{1}{\beta}\sum_{iq_\nu}\tilde{K}^{\parallel}_{3,kmn}\tilde{K}^{\parallel}_{3,lm'n'}\tilde{L}^{h}_{\parallel mm'}(iq_\nu) \times\tilde{L}^{h}_{\parallel,nn'}(i\omega_\nu-iq_\nu)\ . \tag{4.44}$$

Now we can use the double-pole approximation for $\tilde{L}^{h}_{\parallel mn}$ and the definition in (4.42) to obtain

$$S_M(i\omega_\nu)=-\frac{1}{\beta}\sum_{iq_\nu}\sum_{\lambda,\lambda'}(K^{\parallel}_{3,\lambda,\lambda'})^2L^{h}_{\lambda}(iq_\nu)L^{h}_{\lambda'}(i\omega_\nu-iq_\nu)\ , \tag{4.45}$$

where

$$K^{\parallel}_{3,\lambda,\lambda'}=C_{M,k}\tilde{K}^{\parallel}_{3,klm}C_{\lambda,l}C_{\lambda',m}\ . \tag{4.46}$$

Hence, in the double-bond harmonic model the coupling constants to the different modes get renormalized from the values in the single-bond anharmonic model and are also dependent on the mode indices. On comparing (3.16) with (4.45) one finds that these renormalizations are given by

$$g_{\lambda,\lambda'}=\left[\frac{K^{\parallel}_{3,\lambda,\lambda'}}{K^{\parallel}_{M,3}}\right]^2, \tag{4.47}$$

where $K^{\parallel}_3$ has become $K^{\parallel}_{M,3}$ in the notation appropriate to this section. Using the normalization of $C_{\lambda,l}$ in (4.14) and the definition in (4.43) and the explicit result for $K_{I,3}$ in (2.15c) one obtains

$$g_{\lambda,\lambda'}=\left[1+\frac{k_Il_{0M}}{k_Ml_{0I}}C_{M,2}C_{\lambda,2}C_{\lambda',2}\right]^2. \tag{4.48}$$

This renormalization is finite in the limit $k_M/k_I\to\infty$ due to the factor k_M/k_I in $C_{M,2}$; see Eq. (4.27b). In particular, the strength of the Fermi-resonance effects are influenced by g_{RT}. In this situation the renormalized coupling constant $\delta\omega^{\rm eff}_R$ is given by

$$(\delta\omega^{\rm eff}_M)^2=g_{RT}(\delta\omega_M)^2\ . \tag{4.49}$$

By this we mean to indicate that $\delta\omega_M$ in (3.17) is to be replaced by the much smaller $\delta\omega^{\rm eff}_M$. Before giving explicit results for the magnitude of this renormalization of the Fermi-resonance effects for CO on Pt(111), we first generalize the vertex approximation to the double-bond anharmonic model.

D. Generalized effective vertex

Here we generalize the diagrammatic expansion by considering the self-energy S_{kl} defined in (4.40) and its counterpart for the mode M defined in (4.42). This can be done in a compact way by working with the propagator matrices introduced in the corresponding Sec. IV B 1. In this section, we make heavy use of the Einstein summation convention on the bond indices $klmn$ (see Table II).

First, we have to give expressions for a few more vertices besides the cubic vertex defined in (4.43) generated by $H_{\rm int}$ in (4.3). We still have the same kind of vertices as for the single-bond anharmonic model with the main difference being that the vertices are not scalar quantities but rather matrices connecting the different correlation matrices. The cubic interaction couples the L's of the perpendicular modes in the following combination: $\tilde{K}^{\perp}_{3,klm}\tilde{L}^{h}_{\perp,kk'}\tilde{L}^{h}_{\perp,l'l}\tilde{L}^{h}_{\pm,mm'}$ where

$$\tilde{K}^{\perp}_{3,klm}=K^{\perp}_{M,3}\delta_{k1}\delta_{l1}\delta_{m1}+K^{\perp}_{I,3}\delta_{k2}\delta_{l2}\delta_{m2}\ . \tag{4.50}$$

The only quartic term of interest for the effective vertex is the one that couples the parallel and perpendicular modes, which can be written as $\tilde{K}^{\parallel}_{4,klmn}\tilde{L}^{h}_{\perp,kk'}\tilde{L}^{h}_{\perp,l'l}\tilde{L}^{h}_{\parallel,mm'}\tilde{L}^{h}_{\parallel,nn'}$, where

$$\tilde{K}^{\parallel}_{4,klmn}=K^{\parallel}_{4,M}\delta_{k1}\delta_{l1}\delta_{m1}\delta_{n1}+K^{\parallel}_{4,I}\delta_{k2}\delta_{l2}\delta_{m2}\delta_{n2}\ . \tag{4.51}$$

The same kind of diagrammatic argument for the effective vertex both for the dephasing of the M mode and the I mode also goes through in this case for the correlation matrices. The resulting effective vertex is then given by

$$\tilde{K}^{\rm eff,\parallel}_{4,klmn}(i\omega_\nu,ip_\nu,iq_\nu)=\tilde{K}^{\parallel}_{4,klmn}+3\tilde{K}^{\perp}_{3,klq}\tilde{L}^{h}_{\perp,q'q}(ip_\nu+iq_\nu)\tilde{K}^{\parallel}_{3,q'mn}+\tilde{K}^{\parallel}_{3,kmq}[\tilde{L}^{h}_{\parallel,q'q}(i\omega_\nu-ip_\nu)+\tilde{L}^{h}_{\parallel,q'q}(i\omega_\nu-iq_\nu)]\tilde{K}^{\parallel}_{3,q'ln} \tag{4.52}$$

with the same Matsubara frequencies $i\omega_\nu$, ip_ν, and iq_ν.

Here, we are only interested in the dephasing of the stretch mode M, so that in all external solid legs, we get the dominant contribution from the corresponding pole $C_{M,k}C_{M,l}L^{h}_{M}$ in (4.19). Furthermore, since we are considering temperatures where all modes except the dephasing quasimode T are thermally unoccupied, the dominant contribution to the external dashed legs comes from the pole $C_{T,m}C_{T,n}L^{h}_{T}$. Hence, in the evaluation of the self-energy S_M, we are left with a subset of diagrams of propagators L^{h}_{M} and L^{h}_{T} with an effective scalar vertex $\tilde{K}^{\rm eff,\parallel}_4$ given by

$$\tilde{K}^{\rm eff,\parallel}_4(i\omega_\nu,ip_\nu,iq_\nu)=\tilde{K}^{\rm eff,\parallel}_{4,klmn}(i\omega_\nu,ip_\nu,iq_\nu)C_{M,k}C_{M,l}C_{T,m}C_{T,n}\ . \tag{4.53}$$

Now we can evaluate this effective vertex using the normalization in (4.14) and make use of the fact that only the anharmonic terms introduced by U_I that contains single factors of $C_{M,2}$ survive in the limit $k_I/k_M\to\infty$. The resulting effective $\tilde{K}^{\parallel}_4$ is then given by

$$\tilde{K}_4^{\text{eff},\parallel}(i\omega_\nu, ip_\nu, iq_\nu)=K_{M,4}^{\parallel}+3K_{3,M}^{\parallel}\tilde{L}_{\perp,q'1}^{h}(ip_\nu+iq_\nu)\tilde{K}_{3,q'mn}^{\parallel}C_{T,m}C_{T,n}$$
$$+\tilde{K}_{3,kmq}^{\parallel}C_{M,k}C_{T,m}[\tilde{L}_{\parallel,q'q}^{h}(i\omega_\nu-ip_\nu)+\tilde{L}_{\parallel,q'q}^{h}(i\omega_\nu-iq_\nu)]\tilde{K}_{3,q'ln}^{\parallel}C_{M,l}C_{T,n} \ . \quad (4.54)$$

Hence, the only anharmonic force constant introduced by U_I that survives in this limit is $K_{I,3}^{\parallel}$ present in the vertex $\tilde{K}_{3,kml}^{\parallel}$.

Now, we turn to the evaluation of the two first terms on the right-hand side of (4.54). As in the case for the effective vertex in (3.4), we can use the zero-frequency limit of $\tilde{L}_{\perp,kl}^{h}$ in the Matsubara summation over ip_ν and iq_ν. From the result in (4.29), we obtain in this static limit from the two first terms on the right-hand side of (4.54) an effective anharmonic force constant $\mathcal{K}_4^{\parallel,(1)}$ given by

$$\mathcal{K}_4^{\parallel,(1)}=K_{M,4}^{\parallel}-3\frac{K_{3,M}^{\parallel}K_{3,M}}{k_M} \ . \quad (4.55)$$

Inserting the explicit results for the anharmonic force constants $K_{M,4}^{\parallel}$ and $K_{3,M}^{\parallel}$ in (2.15c) in terms of anharmonic coefficients of U_M into (4.55) gives

$$\mathcal{K}_4^{\parallel(1)}=-\frac{K_{2,M}}{2l_{M0}^2} \ . \quad (4.56)$$

Hence, even in this more general anharmonic model the intrinsic anharmonicities of the central forces associated with the two bonds give no contribution to the effective anharmonic force constant and we are left with the results from the minimal anharmonicity model.

Now it remains to evaluate the contribution $\mathcal{K}_4^{\parallel,(2)}$ to the effective anharmonic force constant from the third term on the right-hand side of (4.54). First, we can simplify this term by introducing the exact form for $\tilde{L}_{\parallel,mn}^{h}$ in (4.12) and using the definition in (4.46) as

$$\tilde{K}_{3,kmq}^{\parallel}C_{M,k}C_{T,m}[\tilde{L}_{\parallel,q'q}^{h}(i\omega_\nu-ip_\nu)+\tilde{L}_{\parallel,q'q}^{h}(i\omega_\nu-iq_\nu)]\tilde{K}_{3,q'ln}^{\parallel}C_{M,l}C_{T,n}$$
$$=\tilde{K}_{3,kmq}^{\parallel}C_{M,k}C_{T,m}[\tilde{L}_{\parallel,q'q}^{h,\text{band}}(i\omega_\nu-ip_\nu)+\tilde{L}_{\parallel,q'q}^{h,\text{band}}(i\omega_\nu-iq_\nu)]\tilde{K}_{3,q'ln}^{\parallel}C_{M,l}C_{T,n}$$
$$+(K_{3,RT}^{\parallel})^2[L_R(i\omega_\nu-ip_\nu)+L_R(i\omega_\nu-iq_\nu)] \ . \quad (4.57)$$

Here, the most important difference from the vertex approximation for the single-bond anharmonic model is that we have different coupling constants to the mode R and the mode T in the band. In performing the Matsubara summation and making the analytic approximation, we obtain in a similar way using the high-frequency limit of $\tilde{L}_{\parallel,kl}^{h,\text{band}}(\omega)$,

$$\mathcal{K}_4^{\parallel,(2)}=2\frac{(K_{3,BT}^{\parallel})^2Z_B}{\mu_\parallel\omega_M^2}+\frac{(K_{3,RT}^{\parallel})^2Z_R}{4\mu_\parallel\omega_R}\times\left[\frac{2\omega_+}{\omega^2-\omega_+^2}+\frac{2\omega_-}{\omega^2-\omega_-^2}\right], \quad (4.58)$$

where

$$(K_{3,BT}^{\parallel})^2=C_{M,k}C_{T,m}\tilde{K}_{3,kmq}^{\parallel}B_{\parallel,q'q}\tilde{K}_{3,q'ln}^{\parallel}C_{M,l}C_{T,n} \ . \quad (4.59)$$

Now, we can collect our results for $\mathcal{K}_4^{\parallel,(1)}$ and $\mathcal{K}_4^{\parallel,(2)}$ and obtain an effective coupling constant λ_{eff} of the same form as in (3.11),

$$\lambda_{\text{eff}}=\lambda_0\left[1-g_{BT}Z_B\frac{\mu_\perp}{\mu_\parallel}\right]+\tilde{\lambda}_{\text{Fermi}} \quad (4.60)$$

and where we have in analogy with (4.47)

$$g_{BT}=\left[\frac{K_{3,BT}^{\parallel}}{K_{M,3}^{\parallel}}\right]^2 \quad (4.61)$$

with $K_{3,BT}$ given by (4.59) and

$$\tilde{\lambda}_{\text{Fermi}}=g_{RT}\lambda_{\text{Fermi}} \ . \quad (4.62)$$

The main important difference from the result for λ_{eff} in (3.21) is the presence of the renormalization constants g_{BT} and g_{RT}, defined in (4.47), which we find change drastically our results from those of the single-bond model.

E. Application to CO on Pt(111)

Here, we explicitly consider the results from the double-bond anharmonic model for the coupling constant $\delta\omega_M^{\text{eff}}$ appearing in the Fermi resonance and λ_{eff} for the dephasing. The most important quantities that appear in these coupling constants are the renormalization coefficients g_{BT} and g_{RT} defined in (4.47). Using the results for the various coefficients that determine g_{BT} and g_{RT} in the frozen substrate situation and in the limit of widely separated frequencies, one obtains

$$g_{BT}^{(\infty)}=\left[1+\frac{M_O}{M_O+M_C}\frac{l_{0I}}{l_{0M}}\right]^2, \quad (4.63a)$$

$$g_{RT}^{(\infty)}=\left[\frac{M_C}{M_O+M_C}\right]^2\left[\frac{l_{0I}}{l_{0M}+l_{0I}}\right]^2 . \quad (4.63b)$$

This result for $g_{RT}^{(\infty)}$ shows directly that we expect a large reduction of the Fermi-resonance effect as discussed in Sec. III D for most top-bonded CO molecules due both to a mass factor $M_O/(M_O+M_C)\approx\frac{1}{2}$ and a geometric factor of $l_{0I}/(l_{0I}+l_{0M})\approx\frac{1}{3}$. This reduction is clearly demonstrated by the calculated values of $g_{RT}^{(\infty)}$ and the corresponding $\delta\omega_M^{\text{eff}}$ for the systems in Table I,

	Pt(111)	Cu(100)	Ni(100)	Ir(100)
$g_{RT}^{(\infty)}$	0.024	0.026	0.027	0.025
$\delta\omega_M^{\text{eff}}$	4.0	4.6	7.0	4.4

With the exception of CO on Pt(111), the Fermi-resonance effects are reduced dramatically by these small values for g_{RT}, since $\delta\omega_M^{\text{eff}} \ll |\omega_M-\omega_R-\omega_T|$. The calculated values for the renormalized strength ratios W_{RT}/W_M, as already presented in the Introduction, are negligible. Nor are these small values for g_{RT} an artifact of either the frozen lattice or wide-frequency approximations. For instance, in the full lattice-dynamical calculation for CO on Pt(111), we obtain from the calculated parameters in Table IV that, in fact, $g_{RT}=2\times10^{-6}$ and $\delta\omega_M^{\text{eff}}=5\times10^{-5}$. These are essentially zero and there is no Fermi-resonance effect, despite the near-resonance condition $\omega_M-\omega_R-\omega_T\approx0$.

Now we turn to the effective coupling constant for dephasing, and discuss several different cases. Note first in the limit $\omega_M \gg \omega_R$,

$$\tilde{\lambda}_{\text{eff}}=\lambda_0\left[1-(g_{BT}Z_B+g_{RT}Z_R)\frac{\mu_\perp}{\mu_\parallel}\right]. \tag{4.64}$$

In the wide-frequency and frozen lattice situation one finds that

$$Z_T^{(\infty)}g_{TT}^{(\infty)}+Z_R^{(\infty)}g_{RT}^{(\infty)}=\frac{M_C}{M_O+M_C} \tag{4.65}$$

(note that $Z_B=Z_T$ and $g_{BT}=g_{TT}^{(\infty)}$ in this situation), and so $\tilde{\lambda}_{\text{eff}}=0$. This is the analog of our exact result in the monatomic case. Although the cancellation is not complete in the full lattice-dynamical calculation, where $\tilde{\lambda}_{\text{eff}}\approx-0.06\lambda_0$ for CO on Pt(111), this value is still much less than the corresponding value of $-1.2\lambda_0$ in the single-bond model.

Another straightforward case is the opposite limit $\omega_R \gg \omega_M$, where $\tilde{\lambda}_{\text{Fermi}}=g_{RT}\lambda_{\text{Fermi}}=0$ and

$$\tilde{\lambda}_{\text{eff}}=\lambda_0\left[1-g_{BT}Z_B\frac{\mu_\perp}{\mu_\parallel}\right]. \tag{4.66}$$

This reduces to

$$\tilde{\lambda}_{\text{eff}}=Z_T^{(\infty)}\frac{M_O}{M_O+M_C}\left[\frac{l_{I0}}{l_{M0}}\right]^2\lambda_0 \tag{4.67}$$

in the wide-frequency and frozen lattice situation and is typically much less than the corresponding single-bond value

$$\lambda_{\text{eff}}=Z_T^{(\infty)}\frac{M_O}{M_C}\left[\left[1+\frac{l_{I0}}{l_{M0}}\right]^2-1\right]\lambda_0 \tag{4.68}$$

for the systems in Table I. In the case of CO on Pt(111) the corresponding values are $0.04\lambda_0$ and $0.45\lambda_0$, respectively. This large reduction prevails also in the full lattice-dynamical calculation, where the corresponding value is $-0.06\lambda_0$. Thus, in either of these limits there is an almost complete cancellation of the harmonic contribution to the effective coupling constant in the double-bond model.

The actual values for ω_R for the systems in Table I (Refs. 18–29) are intermediate to these two limits and there is a possibility of having enhanced effective coupling constants due to the resonance denominators in λ_{Fermi}. However, the small value for g_{RT} makes this contribution small, as already discussed above. This effect can be seen by making the wide-frequency and frozen lattice approximations for all terms in λ_{eff}, as given by (4.60). One must take care to include the resonant denominators in λ_{Fermi} correctly, by using (4.62) and (3.24). This yields

	Pt(111)	Cu(100)	Ni(100)	Ir(100)
$\tilde{\lambda}_{\text{eff}}/\lambda_0$	−1.4	−0.15	−0.10	−0.33

The values for the effective coupling constants are no longer preposterously large, as they were in the single-bond model. The value for CO on Pt(111) is relatively large compared to other cases due to the near-resonance condition for $\omega_R=410\ \text{cm}^{-1}$, but as already stressed the experimental uncertainties are too large in this case to get any reliable results. Furthermore, in the full lattice-dynamical calculation the extremely small value for g_{RT} makes $\tilde{\lambda}_{\text{eff}}\approx0$ even for $\omega_R=410\ \text{cm}^{-1}$ which gives a near cancellation of the harmonic part, $\lambda_{\text{eff}}\approx-0.06\lambda_0$.

Finally, LP noted that the observed temperature-dependent shift and broadening for the M mode of CO on Pt(111) are both consistent with a coupling constant of about λ_0. We now find that such a large value cannot be obtained in the double-bond model. Thus, also in this case as for the dephasing of the internal mode I one needs to scrutinize cubic and quartic terms in the small noncentral forces in order to obtain a convincing explanation of the observable dephasing.

V. CONCLUDING REMARKS

One of the interesting questions that arises in the study of vibrational linewidths of adsorbates can be formulated as the following: What kind of information can be obtained about the interatomic forces from the dephasing of an adsorbate? We have found the remarkable result that central forces usually *do not* contribute to the dephasing of a *high-frequency* perpendicular mode of a top-bonded adsorbate. So, unlike the vibrational frequencies themselves whose values are determined largely by the central forces, the dephasing of these modes is presumably dominated by noncentral forces. Therefore the results suggest that the line shape contains information about the non-

central forces, rather than the central forces, as one would naively assume.

The above broad statements are based on several distinct theoretical results. We have shown that central forces do not contribute to dephasing at all whenever the mode being probed has a frequency far above all other modes. This result is based on an effective vertex derived in many-body diagrammatic perturbation theory for the coupling constant for dephasing. In deriving this result, we find that not only the quartic terms in the anharmonicity but also the *cubic terms* play a most important role. In fact, these two contributions cancel to give the final result. This result can also be understood in a simple model without any reference to many-body perturbation theory, just by a coordinate transformation to stretch and angle-bending coordinates. This complete cancellation applies both to H on Si(111) and the internal CO stretch for CO adsorbed on metal substrates, so that we suggest noncentral forces be studied to determine the source of dephasing in both these systems.

For the adsorbate-substrate stretch of a diatomic adsorbate, we see a richer behavior due to the existence of several perpendicular and parallel adsorbate modes. We have therefore been much more specific in doing a detailed analysis of CO adsorbed in an on-top site on the (100) surface of Cu, Ni, and Ir and also on the Pt(111) surface. The adsorbate vibrational structures of all these systems are very similar, and many of the conclusions we arrive at for this class of systems should have a wider range of applicability. By including cubic anharmonicity we find that, if we make the natural assumption that the C-O bond is rigid during the dephasing of the C-metal stretch, strong Fermi resonances appear between the C-metal mode and a combined frustrated translation and rotation. Such resonances lead to both satellites and a greatly enhanced linewidth, but neither have been seen in experiments. In fact, by allowing the internal mode to move, we find the important and surprising result that this motion, despite being very small, has a large impact on the effect of the Fermi resonances. This slight stretch of the internal mode not only makes the satellite strengths negligible, but also drastically reduces the effective coupling for dephasing. This can be seen analytically, by making both the widely separated frequencies and the frozen lattice approximations. We have also shown these approximations to be valid, by checking them with a full surface lattice-dynamical calculation for CO on Pt(111). Finally, if all the parallel modes were at much lower frequencies than the mode being probed, once again the effective coupling vanishes, at least within the frozen lattice approximation, just as in the cases discussed in the previous paragraph. In fact, the central force model for the anharmonicity leads to substantial dephasing *only* if Fermi resonances occur, and they are strong enough to overcome the reduction factor due to the motion of the internal stretch.

ACKNOWLEDGMENTS

We thank Yves Chabal and Prasenjit Saha for fruitful discussions or correspondence. This work was supported in part by the National Science Foundation under Grants No. DMR-88-01027 and DMR-91-03466 and also in part by the Swedish Natural Science Research Council (NFR).

*Present address: Department of Physics, Indiana University, Swain West 117, Bloomington, IN 47405.

[1]B. N. J. Persson and R. Ryberg, Phys. Rev. B **40**, 10 273 (1989).

[2]D. C. Langreth and M. Persson, Phys. Rev. B **43**, 1353 (1991), abbreviated LP.

[3]P. Dumas, Y. Chabal, and G. S. Higashi, Phys. Rev. Lett. **65**, 1124 (1990).

[4]D. Hoge *et al.*, Chem. Phys. Lett. **151**, 230 (1988).

[5]I. J. Malik and M. Trenary, Surf. Sci. **214**, L237 (1989).

[6]C. Hirschmugl and G. Williams (private communication).

[7]S. Chiang *et al.*, Phys. Rev. Lett. **52**, 648 (1984).

[8]The exact density of parallel modes, as found in a full surface lattice-dynamical calculation, for CO on Pt(111) is shown in Fig. 5 of Ref. 2.

[9]Z.-Y. Zhang and D. C. Langreth, Phys. Rev. Lett. **59**, 2211 (1987).

[10]Z.-Y. Zhang, Ph. D. thesis, Rutgers University, 1988.

[11]J. Leiro and M. Persson, Surf. Sci. **207**, 473 (1989), abbreviated JP.

[12]C. J. Hirschmugl, G. P. Williams, F. M. Hoffmann, and Y. J. Chabal, Phys. Rev. Lett. **65**, 480 (1990).

[13]B. N. J. Persson, J. Phys. C **17**, 4741 (1984).

[14]There are actually ten diagrams, as three of those shown are not symmetric, and have counterparts with the external legs reversed. However, as these yield the same algebraic contribution, we include these by simply doubling the contribution of the three shown.

[15]G. D. Mahan, *Many Particle Physics* (Plenum, New York, 1981).

[16]K. Burke, P. Saha, and D. C. Langreth (unpublished).

[17]D. Hoge, M. Tüshaus, E. Schweisser, and A. M. Bradshaw, Chem. Phys. Lett. **151**, 230 (1988).

[18]J. E. Black, F. C. Shanes, and R. F. Wallis, Surf. Sci. **133**, 199 (1983).

[19]A. M. Lahee, J. P. Toennies, and Ch. Wöll, Surf. Sci. **177**, 371 (1988).

[20]H. Steininger, S. Lehwald, and H. Ibach, Surf. Sci. **123**, 264 (1982).

[21]S. Andersson, Surf. Sci. **89**, 477 (1979).

[22]B. F. Mason, R. Caudano, and B. R. Williams, Phys. Rev. Lett. **47**, 1141 (1981).

[23]C. J. Hirschmugl, G. P. Williams, and F. M. Hoffmann, Phys. Rev. Lett. **65**, 480 (1990).

[24]S. Andersson and J. B. Pendry, Phys. Rev. Lett. **44**, 363 (1979).

[25]G. Kisters, J. G. Chen, S. Lehwald, and H. Ibach, Surf. Sci. **245**, 65 (1991).

[26]S. Lehwald, J. G. Chen, G. Kisters, E. Preuss, and H. Ibach, Phys. Rev. B **43**, 3920 (1991).

[27]R. Berndt, J. P. Toennies, and Ch. Wöll, J. Electron. Spectrosc. Relat. Phenom. **44**, 183 (1987).

[28]S. Chiang, R. G. Tobin, P. L. Richards, and P. A. Thiel, Phys. Rev. Lett. **52**, 648 (1984).

[29]S. Andersson, Solid State Commun. **21**, 75 (1977).